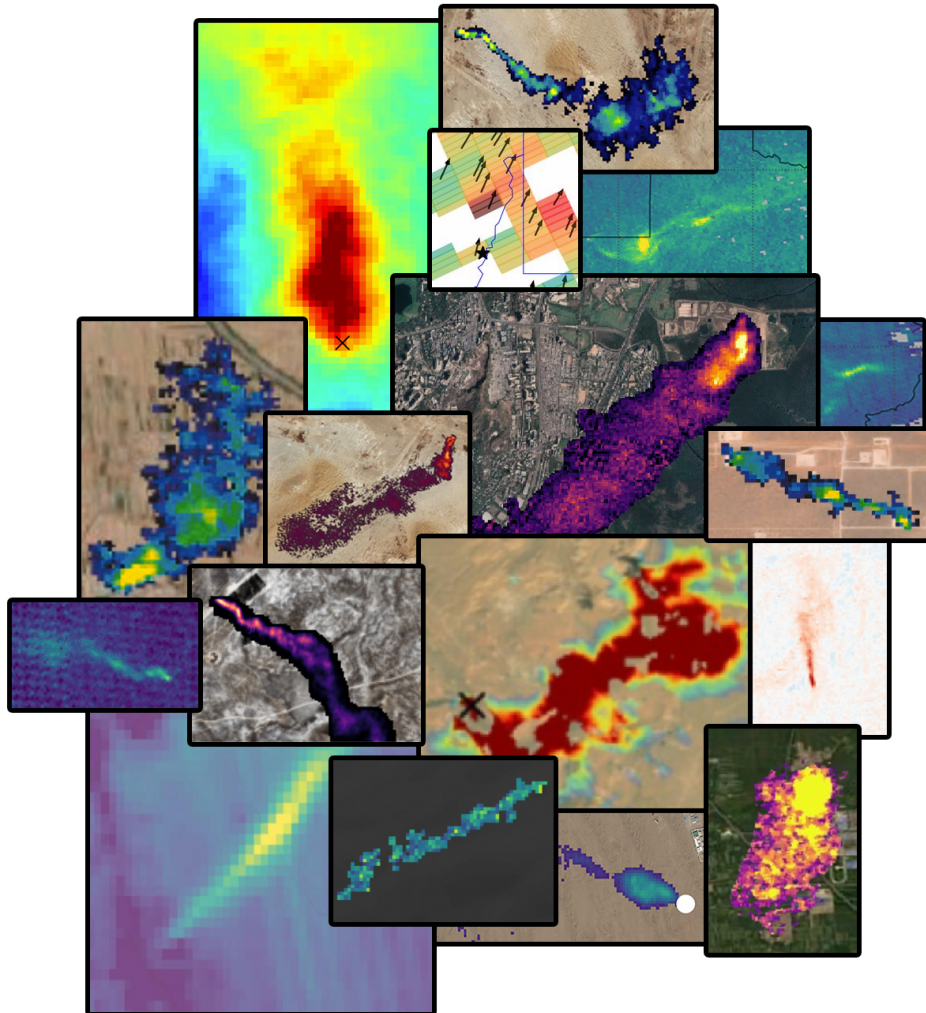


Review of the State-of-the-Art

WP120 - Deliverable D1.2



Authors

Research Institute of Water and Environmental Engineering (IIAMA), Universitat Politècnica de València (UPV)

- Luis Guanter (WP120 & document lead)
- Javier Roger
- Javier Gorroño

SRON Netherlands Institute for Space Research

- Matthieu Dogniaux
- Ilse Aben
- Joannes D. Maasackers

Institute of Environmental Physics (IUP), University of Bremen

- Michael Buchwitz

Kayrros SAS

- Alexis Groshenry
- Julian Akani Guery

Royal Belgian Institute for Space Aeronomy (BIRA)

- Bavo Langerock

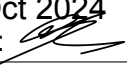
GHGSat

- Antoine Ramier

Change log

Version	Date	Status	Authors	Reason for change
0.1	30-July-2024	Draft	see Authors list	New document
1.0	7-Oct-2024	Final version submitted to ESA	see Authors list	Internal review

Approved by

Date: 7 Oct 2024 Signature: 	Date: Signature:
Dr. Ilse Aben Science Lead SRON	Dr. Simon Pinnock ESA Technical Officer

Contents

1	Preface	7
2	Review of methane-sensitive satellite missions	7
2.1	High-resolution point-source imagers	8
2.1.1	Hyperspectral imagers	8
2.1.2	Multispectral imagers	9
2.1.3	Upcoming high-resolution missions	10
2.2	Global flux mapping missions	11
2.2.1	Sentinel-5P TROPOMI	11
2.2.2	GOSAT(-2)	11
2.2.3	Upcoming flux mapping missions	12
3	Review of methane retrieval and quantification methods for plume imagers	13
3.1	Methane concentration retrieval methods	13
3.1.1	Hyperspectral methane concentration retrieval methods	13
3.1.2	Multispectral ΔXCH_4 retrieval methods	17
3.2	Estimation of emission rates from methane concentration data	18
3.3	Machine learning-based methods for plume detection and quantification	20
3.4	Validation of emission rate estimates and plume detection limits	22
4	Review of methane retrieval and quantification methods for global flux mappers	22
4.1	Methane concentration retrievals	22
4.1.1	Operational TROPOMI XCH_4 product, RemoTeC/SRON	24
4.1.2	WFMD/Bremen	25
4.1.3	Blended TROPOMI+GOSAT satellite data product	26
4.2	Emission detection and quantification methods	26
4.2.1	Plume detection methods for a known source	26
4.2.2	Automatic plume detection by machine learning	27
4.2.3	Plume-based quantification methods	27
4.2.4	Methods relying on multiple TROPOMI overpasses	29

5	Review of available online methane data portals	32
6	Review of methane-related activities of relevance to MEDUSA	33
7	References	36

1 Preface

This document results from the workpackage 120, “Review of the State-of-the-Art”, of the *Methane Emissions Detection Using Satellites Assessment* (MEDUSA) project. It describes the current scenario on the use of satellites for the remote sensing of anthropogenic methane emissions, with emphasis on point sources.

The document is structured in 5 major sections following this preface: Section 2 reviews existing and planned satellite missions with ability for the detection and quantification of methane plumes; Section 3 and 4 describe data processing methods for the retrieval and quantification of methane plumes from space, with focus on either high-resolution satellites or global flux-mapping missions, respectively; Section 5 lists existing methane data portals disseminating information of methane point sources; finally, Section 6 discusses existing methane-related projects and activities which may have synergies with MEDUSA.

2 Review of methane-sensitive satellite missions

Our ability to use satellites for the detection, quantification and monitoring of methane super-emissions has seen a rapid evolution in the last years. Crucial developments in this field have been the advent of a number of methane-sensitive missions with a sufficient spatial resolution to detect and quantify individual methane plumes (Jacob et al., 2022), as well as methodological advances enabling the use of Sentinel-5P/TROPOMI data for the identification of large methane plumes and hotspot regions (Lauvaux et al., 2022; Schuit et al., 2023). As a result, the group of methane-sensitive satellites is currently highly heterogeneous in terms of their detection limits and spatio-temporal sampling.

In the remaining of this section, we discuss available satellite missions for the detection, quantification, and monitoring of methane emissions. We restrict ourselves to super-emitting point sources, including those from the fossil fuel sector, coal mining, and landfills. We opt for a qualitative discussion focused on the potential and limitations of each mission for point source detection and monitoring. The reader is referred to Jacob et al. (2022) and CEOS' Greenhouse Gas Satellite Missions portal¹ for a broader list of methane-capable missions, including those dealing with global fluxes and biogenic sources.

Following the classification by Jacob et al. (2022) used in MEDUSA, we distinguish between high-spatial resolution “point-source imagers” (either hyperspectral or multispectral instruments) and global “flux-mappers”, currently represented by TROPOMI. This classification responds to trade-offs in spatio-temporal sampling and retrieval precision. A summary table including the core satellite missions in MEDUSA is presented in Table 1.

¹<https://database.eohandbook.com/ghg/>

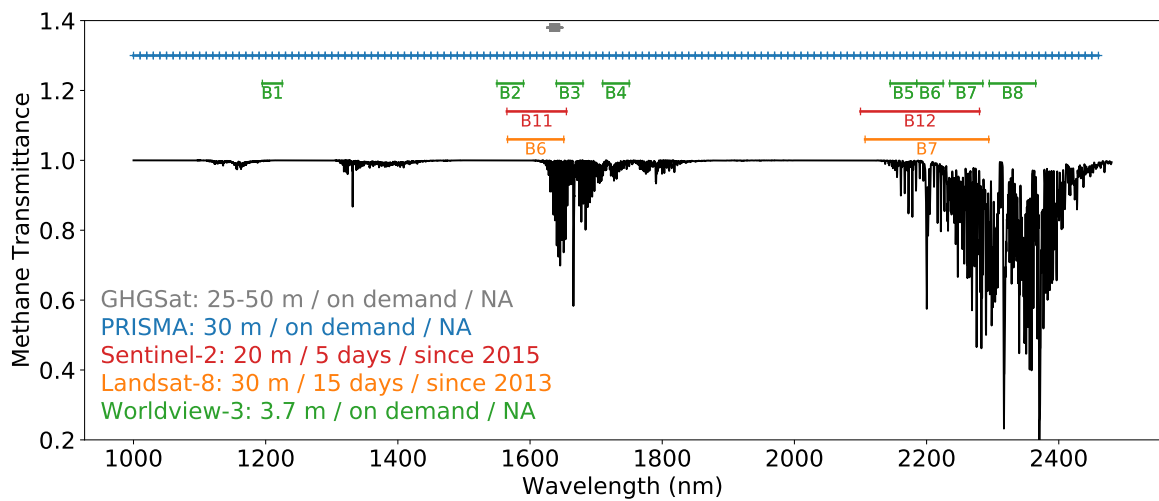


Figure 1: Details of the spectral, spatial and temporal sampling of different point-source imaging missions (from Sánchez-García et al. (2022)).

2.1 High-resolution point-source imagers

Point source imagers generate maps of methane concentrations at a high spatial resolution (typically 20–50 m pixel size), which enables the detection and quantification of methane plumes, and the attribution of these plumes to individual point sources. Depending on their spectral sampling, we can distinguish between hyperspectral and multispectral imagers (see Fig. 1). Hyperspectral imagers have relatively low plume detection limits, but also a poor spatio-temporal sampling, whereas multispectral imagers do offer a frequent global coverage, but their sensitivity to methane is lower than those of hyperspectral instruments.

2.1.1 Hyperspectral imagers

Hyperspectral imagers, also known as imaging spectrometers, offer a high sensitivity to methane through a dense spectral sampling of methane absorption features in the shortwave infrared part of the spectrum. These satellite instruments combine this adequate spectral sampling of methane absorption features with a relatively high spatial sampling of 25–60 m. This configuration enables the detection of plumes in the range of 100–500 kg/h over a relatively wide range of surface types and also the attribution of these plumes to their sources at the facility level. The main limitation of these missions for operational methane mapping and point-source detection is that their spatio-temporal sampling is sparse. Hyperspectral missions typically acquire data under request, so they do not provide global coverage and can not be used for the continuous monitoring of sites over time.

The hyperspectral missions which are currently being most widely used for methane mapping are:

- **GHGSat**: it is a commercial satellite constellation specifically designed for methane mapping, with 12 satellites in orbit at the moment. It combines a high sensitivity to methane with a low sensitivity to the surface and a high spatial sampling. The detection limit is in the range of 100-200 kg/h under favorable conditions (Varon et al., 2020; Jervis et al., 2021). The Fabry-Pérot spectrometers onboard the GHGSat satellites sample the 1700 nm methane band with a high spectral resolution about 0.1 nm, a swath of ~12 km, and a spatial sampling of either 50 or 25 m (Jervis et al., 2021). Acquisitions are commercially available or subject to especial arrangements with GHGSat or other institutions (e.g. ESA's Third Party Mission programme).
- **EnMAP** (DLR/GFZ) and **PRISMA** (ASI): These imaging spectrometers, a different class of instrument than GHGSat, cover most of the solar spectrum (~400–2500 nm) with a typical spectral resolution of 10 nm, and a 30 m spatial sampling. Even though they are not optimized for methane mapping, they sample the strong methane absorption at 2300 nm with tens of spectral channels, which is being exploited for methane retrieval, leading to detection limits of 500-1000 kg/h. These missions have an open data policy, but acquisitions are sparse (Guanter et al., 2021; Roger et al., 2024b).
- **EMIT** (NASA): It is an open-access scientific imaging spectroscopy mission similar to PRISMA and EnMAP. EMIT's coarser spatial resolution (60 m) is partly compensated by its high signal-to-noise ratio. Another difference with respect to EnMAP and PRISMA is that EMIT has a continuous spatial sampling of the latitude belt covered by the International Space Station, rather than operating on a per-site basis (Thorpe et al., 2023).
- **Gaofen-5 AHSI** (and other AHSI versions, from several Chinese institutions): it is one of the most powerful imaging spectroscopy missions for methane mapping due to its wide swath (60 km) and high sensitivity to methane, which is enabled by a spectral resolution about 8 nm at a 30-m sampling (Irakulis-Loitxate et al., 2021). However, the data are in general not available to the international community.

2.1.2 Multispectral imagers

Multispectral imagers are much less sensitive to methane than hyperspectral missions because of the substantially poorer spectral sampling (typically, 1-2 spectral channels covering the 2300 nm spectral region, as shown in Fig. 1). Their methane retrievals are therefore strongly affected by the surface background, which limits its coverage to spatially-homogeneous and bright surfaces, such as those in semi-arid regions. However, thanks to its continuous global coverage and high temporal sampling, multispectral missions can be used for the continuous monitoring over time of strong sources in those regions. The archives of multispectral missions are open, so the generation of retrospective emission time series is possible.

The multispectral missions which are currently being used for methane mapping are:

- **Sentinel-2** (Copernicus/ESA) and **Landsat** (USGS/NASA): They provide wall-to-wall global coverage with a 20-30 m spatial resolution every 2-3 days combining Sentinel-2 (5-days) and Landsat-8/9 (16-days each). These missions are mostly being used to detect and monitor point sources in semi-arid areas (e.g. Varon et al., 2021; Irakulis-Loitxate et al., 2022), where emissions in the range of 10,000 kg/h can be typically detected (Gorroño et al., 2023).
- Medium-resolution multispectral radiometers with sub-daily resolution - **Sentinel-3/SLSTR** (Copernicus/ESA) and **Suomi-NPP/VIIRS** (NOAA): These missions have a similar measurement principle as Sentinel-2 and Landsat, but with a different spatio-temporal sampling combining a medium spatial resolution (300-750 m per pixel) with a high temporal resolution (daily global coverage or better, depending on latitude) (Pandey et al., 2023; de Jong et al., 2024).
- Geostationary missions - **GOES-ABI** (NOAA) and **MTG-FCI** (Eumetsat): They offer a similar methane retrieval principle than the previous multispectral imagers, but the geostationary orbit allows to monitor large methane leaks with a very high temporal resolution of 5-10 min. Detection limits are substantially higher than those of other point source imagers, being in the range of 100,000 kg/h for GOES-ABI (Watine-Guiu et al., 2023); the MTG-FCI is currently on commissioning phase and its potential for methane mapping still needs to be investigated.
- **WorldView-3 SWIR**: multispectral mission with very high spatial resolution (3.5-7 m) and sensitivity to methane from several narrow spectral channels in the 2300 nm region. It is a commercial mission and acquisitions are on-demand, opposed to the other multispectral missions (Sánchez-García et al., 2022).

2.1.3 Upcoming high-resolution missions

Several point-source imaging missions will be launched in the next years, including:

- **Carbon Mapper Tanager-1**: it is an imaging spectroscopy mission similar to EMIT, but with a higher sensitivity to methane thanks to a 5-nm spectral sampling, an enhanced signal-to-noise ratio, and a 30-m spatial sampling. It will also have a higher acquisition capability over relevant methane emission hotspot areas. Launch was on 17 August 2024 and the mission is currently in commissioning phase (Carbon Mapper Inc., 2021).
- **Long-term launches of point-source imagers (~2030)**: **CHIME** (Copernicus/ESA) and **SBG** (NASA) will be imaging spectroscopy missions with a spatio-temporal sampling similar to the current Landsat (global coverage every 2-3 weeks); **Landsat-Next** and **Sentinel-2 NG** will be the new versions of the current Landsat and Sentinel-2, with improved sensitivity to methane and spatio-temporal sampling.

- **Copernicus Contributing Missions: AbsolutSensing** and **Satlantis' GEI-SAT** high resolution missions (an imaging spectrometer and a WorldView-3-like very high resolution mission, respectively) are expected to start operations in 2024-2025. The **AIRMO** mission, combining a spectrometer with a micro-lidar, may join this group of methane-capable missions in the Copernicus Contributing Missions programme in 2025.
- **TANGO:** The Twin Anthropogenic Greenhouse Gas Observers (TANGO) mission is a Cube-sat satellite mission from ESA's SCOUT program comprising two agile satellites: TANGO-Carbon and TANGO-Nitro. The first one will have sensitivity to moderate and strong methane point sources through the sampling of the 1600 nm absorption at a $300 \times 300 \text{ m}^2$ sampling. Launch is expected for 2026.

2.2 Global flux mapping missions

2.2.1 Sentinel-5P TROPOMI

The TROPOspheric Monitoring Instrument (TROPOMI, Veefkind et al., 2012) aboard ESA Sentinel-5P is a push-broom spectrometer with a swath width of 2600 km that provides daily global maps of XCH₄ at $5.5 \times 7 \text{ km}^2$ resolution at nadir. Its observations are taken at 13:30 local time and are publicly available from the operational product with a latency of a few days. Thanks to these characteristics, TROPOMI is the reference mission for daily and systematic surveillance of large plumes around the world and for the identification of hot-spot emission regions (Lauvaux et al., 2022; Maasackers et al., 2022b; Schuit et al., 2023). However, its relatively coarse spatial resolution results in a rather high plume detection threshold $\sim 8 \text{ t/h}$ (Schuit et al., 2023) and limits its ability to be used to precisely determine the emission source.

2.2.2 GOSAT(-2)

The Japanese Greenhouse gases Observing SATellite (GOSAT) was launched in 2009 and has been providing, since then, XCH₄ estimates retrieved from high spectral resolution measurements in the shortwave infrared band near $1.65 \mu\text{m}$ made using its TANSO-FTS instrument (Thermal And Near infrared Sensor for carbon Observation - Fourier Transform Spectrometer). It provides very sparse spatial sampling, observing three across-track 10 km-diameter footprints separated by 260 km (Inoue et al., 2016) and returning to the same observation spots every three days. GOSAT was followed in 2018 by GOSAT-2, which has similarly sparse spatial sampling characteristics (Imasu et al., 2023). Because of this sparse sampling, GOSAT(-2) are not ideal instruments to image methane emission plumes arising from super-emitters.

2.2.3 Upcoming flux mapping missions

Several flux mapping missions with strong potential for methane remote sensing will be launched in the next years, including:

- **MethaneSAT (Environmental Defense Fund)**: it will offer a unique combination of very high measurement precision, thanks to the high spectral sampling of the 1600 nm methane absorption, with a relatively high spatial sampling (100×400 m pixel). This configuration enables the use of MethaneSAT to generate both area- and point-source data products, which will be openly available (Environmental Defense Fund, 2021). MethaneSAT was launched on 4 March 2024, and the public release of the first data is expected for beginning of 2025.
- **Sentinel-5 (Copernicus)**: The Sentinel-5 mission, expected to launch in 2026, will have observations characteristics close to the ones of Sentinel-5P TROPOMI, with measurements in an additional methane-sensitive spectral band near 1650 nm. This additional spectral coverage allows using the CO₂-proxy method to retrieve methane, which is less sensitive to artefacts and can therefore allow greater coverage (Schepers et al., 2012). Sentinel-5 will provide daily global coverage at 9:30 local time with a spatial resolution at nadir of 7.5×7.5 km².
- **GOSAT-GW (NIES/JAXA/MOE)**: The Global Observing Satellite for Greenhouse gases and Water cycle (GOSAT-GW), expected to launch in 2025, will provide observations of XCH₄ retrieved from measurements in the 1650 nm methane band with 0.2 nm spectral resolution at 13:30 local time. Its nominal observation mode will comprise a ~1000 km swath with 10×10 km² pixel resolution (resulting in global coverage every three days), but a focused target mode with a 1×1 km² pixel resolution will also be available.
- **CO2M (Copernicus)**: the CO₂M mission will consist of two satellites with capability to measure carbon dioxide, nitrogen dioxide and methane in support of estimating anthropogenic emissions. The spectrometers in CO₂M will have a relatively high spatial resolution of 4 km and an 11-day repeat cycle. The 1590–1675 nm window will be used for methane retrievals. The launch of the first satellite is planned for 2026.

Table 1: Key characteristics of currently-operating satellite instruments used for plume detection and quantification tasks in MEDUSA. Grades range from -- (top weakness) to ++ (top strength).

	Detection limit	Revisit time	Spatial res.	Spectral res.	Coverage	Data access	Methane product
GHGSat	++	++	++	++	Per Site	Private	Plume, flux
EnMAP PRISMA	+	-	++	-	Per Site	Open	No
EMIT	+	-	+	-	Wall-to-wall (ISS orbit)	Open	Plume
Sentinel-2 Landsat-n	-	+	++	--	Wall-to-wall	Open	No
SLSTR VIIRS	--	++	--	--	Wall-to-wall	Open	No
GOES ABI MTG FCI	--	++	-	--	Americas or Europe-Africa	Open	No
TROPOMI	-	++	--	++	Wall-to-wall	Open	XCH ₄

3 Review of methane retrieval and quantification methods for plume imagers

3.1 Methane concentration retrieval methods

3.1.1 Hyperspectral methane concentration retrieval methods

Since high-resolution satellite instruments are commonly used to detect and quantify individual methane sources, the target variable of methane retrievals for those missions is typically the per-pixel enhancement of methane column concentration with respect to the background (ΔXCH_4) caused by those sources.

Both data-driven and physics-based methods have been used for ΔXCH_4 retrieval with imaging spectroscopy data:

- Data-driven methods are based on statistical approaches that convert spectral anomalies in the 2300 nm spectral window into a ΔXCH_4 estimate. For example, data-driven methane retrievals based on the matched-filter and the singular vector decomposition concepts have been successfully used with imaging spectroscopy data (Thorpe et al., 2014; Thompson et al., 2015, 2016; Foote et al., 2020).

- physics-based methods rely on the explicit modelling of the radiative transfer between the surface, the atmosphere, and the instrument. The family of differential optical absorption spectroscopy (DOAS) methods belong to this group and have been used with AVIRIS and AVIRIS-NG airborne data (e.g. Thorpe et al., 2017; Borchardt et al., 2021). They normally generate maps of the total methane concentration, from which ΔXCH_4 can be inferred through the removal of the background concentration.

Data-driven methods are currently being more widely used for the processing of the EnMAP, PRISMA and EMIT satellite data with a reduced spectral resolution, whereas a physics-based retrieval is used for GHGSat. The main reasons for favouring data-driven retrievals are that they are of simpler implementation, computationally-efficient, and can implicitly account for potential radiometric and spectral errors, which are likely to happen in satellite imaging spectroscopy data.

Several data-driven and physics-based methane retrievals are discussed hereinafter in this section.

Matched-filter retrieval

Among data-driven methods, the one based on the matched-filter concept (e.g. Thompson et al., 2016; Foote et al., 2020) is currently the most widely used for the processing of hyper-spectral data. This retrieval relies on the idea that each input spectrum can be expressed as a mean spectrum plus its perturbation by a change in the methane column concentration. This is modelled as a so-called target spectrum, which represents the radiative transfer signal of a unit methane absorption.

The matched-filter concept for the retrieval of ΔXCH_4 from spaceborne hyperspectral data was first proposed by Thompson et al. (2016). In their formulation, $\hat{\alpha}$ was ΔXCH_4 (in parts-per-billion, ppb), and the matched-filter takes the form

$$\hat{\alpha}(\mathbf{x}) = \frac{(\mathbf{x} - \boldsymbol{\mu})^T \boldsymbol{\Sigma}^{-1} \mathbf{t}}{\mathbf{t}^T \boldsymbol{\Sigma}^{-1} \mathbf{t}}, \quad (3.1)$$

where \mathbf{x} is the spectrum under analysis, $\boldsymbol{\mu}$ and $\boldsymbol{\Sigma}$ are the mean and covariance of the background radiance, and \mathbf{t} is the target spectrum representing the perturbation of the background radiance signal by a methane enhancement. The \mathbf{t} spectrum has units of radiance over methane column concentration, and is generated as the element wise multiplication of $\boldsymbol{\mu}$ and \mathbf{k} , with \mathbf{k} being a unit methane absorption spectrum, that can be extracted from HITRAN (Kochanov et al., 2016) or from radiative transfer simulations with e.g. the MODTRAN radiative transfer code (Berk et al., 2014).

An example of a \mathbf{k} target unit absorption spectrum is shown in Fig. 2. The variables $\boldsymbol{\mu}$ and $\boldsymbol{\Sigma}$ (empirical covariance) are typically calculated on a per-detector-column basis in order to account for the different radiometric responses of detector elements across-track. The 2110–2450 nm window offers a good compromise between retrieval precision and systematic errors.

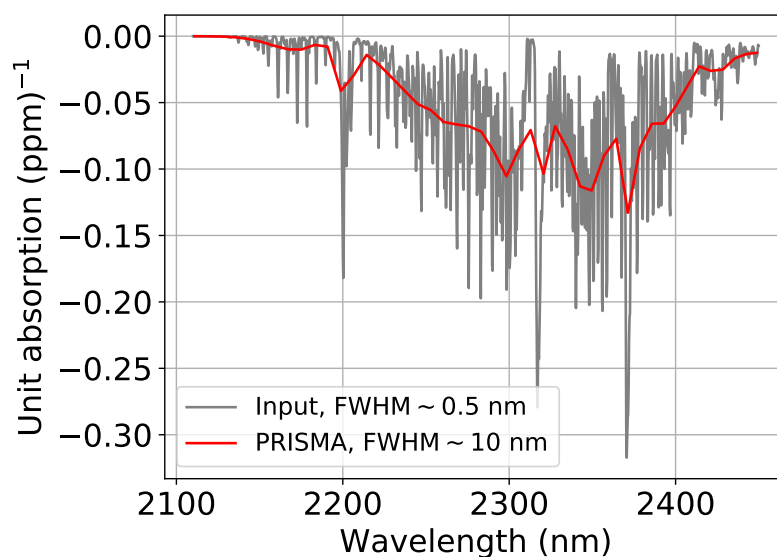


Figure 2: Example of a unit methane absorption spectrum k used as target signature for the processing of PRISMA data by the matched-filter retrieval method implemented at the UPV-LARS group (from Guanter et al., 2021).

The sensitivity analysis presented by Guanter et al. (2021) showed that the matched-filter retrieval performs satisfactorily with PRISMA data over many sites characterized by strong point emissions. However, this study also reveals the relatively large dependence of the retrieval on the surface properties. Whereas $1\text{-}\sigma$ retrieval errors of ~ 60 ppb were found for a homogeneous surface in Algeria, the same errors can be up to 3 times higher at a heterogeneous mining site in China. This situation is illustrated by the ΔXCH_4 maps displayed in Fig. 3.

It must be remarked, however, that this sensitivity to the surface and the subsequent high amount of false plume positives in the resulting ΔXCH_4 maps is not intrinsic to matched-filter retrievals, but caused by the relatively-coarse spectral resolution of hyperspectral data, which limits our ability to disentangle methane and surface spectral signals.

Advanced versions of the classical matched-filter retrieval

Different implementations of the matched-filter ΔXCH_4 retrieval have been proposed in order to improve its sensitivity to surface structures and ΔXCH_4 quantification skills:

- **MAG1C:** The Matched filter with Albedo correction and reweighted L1 sparsity Code (MAG1C) (Foote et al., 2020) performs an albedo correction on the radiance L1 data to account for the homogeneity assumption of the matched filter. Additionally, it leverages the methane sparsity assumption by applying an iterative regularization to minimize background noise.
- **ILMF:** The Iterative Lognormal Matched Filter (ILMF) (Pei et al., 2023) uses the logarithm of the L1 radiance cube as input data instead of directly the radiance to overcome the underestimation resulting from the matched filter linear approximation of the methane absorption,

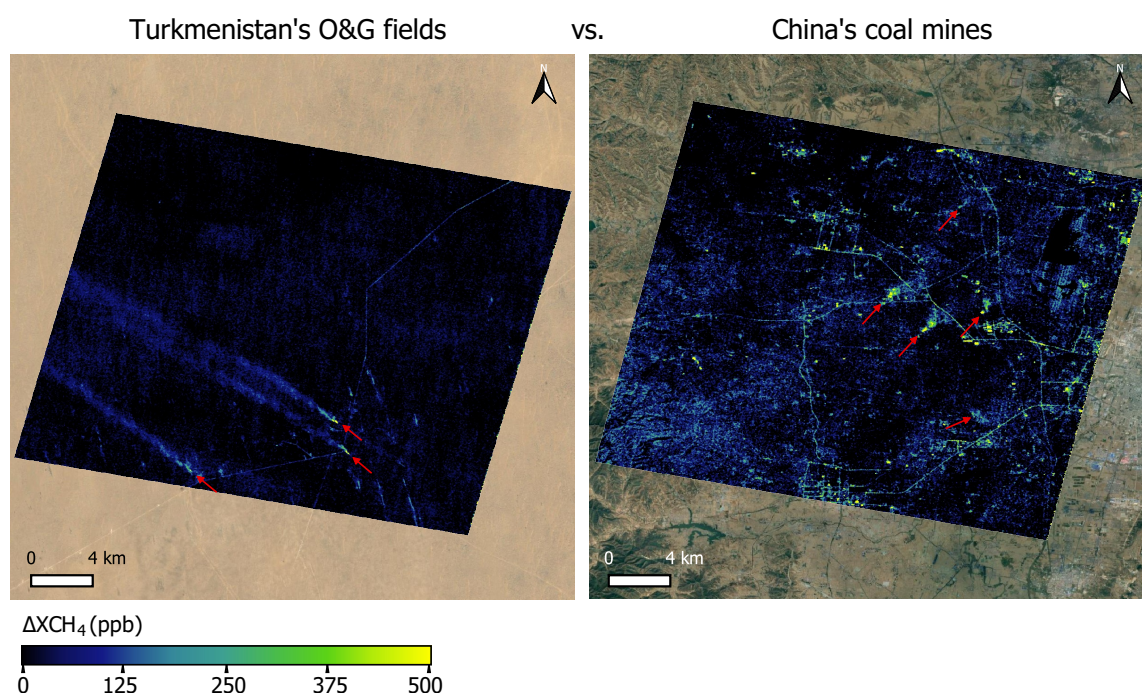


Figure 3: Illustration of the impact of the surface brightness and homogeneity on ΔXCH_4 retrievals from PRISMA hyperspectral data. Left, clear plumes are visible across several kilometers in an oil and gas (O&G) extraction site in Turkmenistan, where the surface is highly homogeneous. Right, the confounding effects of surface structures on the retrieval are evident in the China coal mining site, where the surface is relatively heterogeneous.

since this approach is only accurate enough for relatively weak plumes. This method also accounts for an albedo correction and an iterative process to reduce the contamination of the mean and covariance values due to the existence of retrieval artifacts and random noise.

- **Combo-MF:** The Combo Matched Filter (Combo-MF) (Roger et al., 2024a) exploits a wide spectral range in the shortwave infrared region (1000-2500 nm), aiming to reduce the occurrence of retrieval artifacts and background noise to improve methane plume detection.
- **Model Adjusted Matched Filter:** it uses an adjustment coefficient in order to reduce the fraction of false detections compared to the Matched Filter (MF) without preventing the detection of plumes (Ouerghi et al., 2024).

Other methane concentration retrieval approaches used with high resolution spectrometers

- **SVD-based retrieval:** Another data-driven methane concentration retrieval method is the one based on the singular value decomposition (SVD) concept. This method relies on

a series of orthogonal spectral vectors and a methane Jacobian to model the at-sensor radiance spectrum (Thorpe et al., 2014). The weights of the singular vectors and of the methane Jacobian are inverted through a linear fit of the at-sensor radiance spectrum, with the weight of the methane Jacobian being related to methane concentration. The SVD retrieval method was first applied to AVIRIS by Thorpe et al. (2014), and then to PRISMA by Joyce et al. (2023). However, the advantages of the SVD retrieval with respect to the matched filter remain unclear, and the latter is much more widely used in the literature.

- **GHGSat retrieval:** Methane concentrations are derived from GHGSat at-sensor radiance spectra using a physics-based retrieval. A forward model combining an instrument model and an atmospheric model is used to generate at-sensor radiance spectra. Surface albedo and the vertical column density of carbon dioxide, methane and water vapor are included in the state vector of this forward model. This is inverted using an optimal estimation framework and an iterative Gauss-Newton minimisation procedure applied to the whole scene, followed by the inversion of a linearized forward model applied on a per-pixel basis (Jervis et al., 2021).
- **DOAS-based physics-based retrievals** An iterative maximum a posteriori differential optical absorption spectroscopy retrieval method (IMAP-DOAS) was proposed for AVIRIS and AVIRIS-NG in early works (Thorpe et al., 2014, 2017). The IMAP-DOAS retrieval is a physics-based retrieval in which a per-pixel methane volume mixing ratio can be inferred from the inversion of a forward model including instrument, surface and atmospheric gas variables in the state vector, similar to the GHGSat retrieval described previously. An IMAP-DOAS retrieval was also assumed by Cusworth et al. (2021) in their satellite-based sensitivity analysis. This type of retrieval has the advantage with respect to data-driven methods of not relying on scene statistics. As its main shortcoming is the relatively high computation time. The weighting function modified differential optical absorption spectroscopy (WFM-DOAS) retrieval proposed by Borchardt et al. (2021) for AVIRIS-NG was intended to alleviate this limitation. It consisted of a first order Taylor series approximation of the Lambert–Beer law using only one precalculated radiative transfer calculation per scene.

3.1.2 Multispectral ΔXCH_4 retrieval methods

As opposed to imaging spectrometers, multispectral instruments do not resolve the entire SWIR spectral region; however, several multispectral missions include spectral channels in the SWIR methane absorption region around 2300 nm. It is the case of the B12 channel in Sentinel-2 mission, and the B7 channel in Landsat-7/8/9 (see Fig. 1). Also the medium-resolution multispectral instruments VIIRS and SLSTR, and the GOES-ABI and MTG-FCI instruments, share this spectral configuration enabling methane retrievals.

The rationale to detect methane plumes with these multispectral instruments is that of normal-

ising the radiance at the spectral channel affected by methane absorption by a “methane-free” reference band, which can be a different band with a weaker impact of methane (multi-band approach) or the same band from a different acquisition (multi-temporal approach). Varon et al. (2021) proposed both mono and multi-temporal ΔXCH_4 retrieval approaches for Sentinel-2, retrieving methane column enhancements by exploiting B11 (methane-free reference band) and B12 (methane-sensitive band). Their results show that the combination of both multi-spectral and multi-temporal information leads to the best solution. In that case, the ratio of B12 and B11 enhances the methane plume signal and, the normalisation of the B12/B11 ratios from two consecutive acquisitions helps to cancel out the interference of surface patterns.

The quantification of these methane emissions is based on establishing a relationship between the normalised radiance and the methane enhancement. The normalised radiance is here considered as an approximation of the methane plume transmittance. From the Beer-Lambert law, the relationship can be expressed as

$$\Delta XCH_4 = -\frac{\log(L/L_{ref})}{AMF \sigma_{CH_4}}, \quad (3.2)$$

where L and L_{ref} represent the radiance of the methane-sensitive band and the methane-free reference band, respectively. AMF refers to the air mass factor, and σ_{CH_4} refers to the methane absorption cross section.

The retrieval of ΔXCH_4 with the coarser resolution instruments (SLSTR, VIIRS, GOES-ABI, MTG-FCI) rely on similar approaches combining band ratios between spectral channels at 1600 and 2300 nm and multi-temporal analysis to reduce the impact of the surface background.

3.2 Estimation of emission rates from methane concentration data

After the retrieval of ΔXCH_4 maps, the next step in the processing is the detection and quantification of methane plumes. A comprehensive review of point source quantification methods is provided in Jacob et al. (2022). In general, these methods rely on a mass-balance concept. They model the methane concentration enhancements caused by single point sources. This modelling uses methane concentration maps, plume masks and wind information as input, and allow the estimation of the source emission rate (Q), or the mass of methane emitted by the source per unit time. The most widely-used method for plume quantification with high-resolution satellite data is the integrated mass enhancement (IME) method (Frankenberg et al., 2016; Varon et al., 2018), followed by the cross-sectional flux (CSF) method (Krings et al., 2011).

Flux rate quantification with the IME method

The IME concept was first introduced by Frankenberg et al. (2016) for aircraft measurements, and first applied to satellite data by Varon et al. (2018). The total mass enhancement in the plume is related to the magnitude of emission with a parameterisation dependent on wind speed. This

model calculates an IME in kg units as the total excess mass of methane contained in the plume,

$$\text{IME} = k \sum_{i=1}^{n_p} \hat{\alpha}(i), \quad (3.3)$$

where $\hat{\alpha}$ is the per-pixel methane concentration enhancement, n_p is the number of pixels in the plume and k is a scaling factor which converts the total of pixel-wise methane concentration values in ppb to kg by assuming Avogadro's law and taking into account the pixel size (e.g., $k = 5.155 \cdot 10^{-3}$ kg/ppb for a 30 m pixel). Q is then calculated as

$$Q = \frac{U_{\text{eff}} \cdot \text{IME}}{L}, \quad (3.4)$$

where U_{eff} is an effective wind speed and L the plume length scale in m, which is typically approximated by the square root of the plume mask area. Regarding U_{eff} , this term is intended to account for turbulent diffusion of the methane flux, and also for the fraction of the plume which is not detected due to retrieval noise (Varon et al., 2018). U_{eff} can be expressed as a linear or logarithmic function of the measurable 10-m wind speed U_{10} . This function can be defined with plume simulations including the corresponding spatial sampling and retrieval noise of each instrument. For example, the linear relationship

$$U_{\text{eff}} = 0.33 \cdot U_{10} + 0.45 \quad (3.5)$$

was derived using large-eddy simulations specifically performed for a spatial resolution and ΔX_{CH_4} retrieval precision compatible with Sentinel-2 data by Varon et al. (2020); a similar expression was used for PRISMA by Guanter et al. (2021).

It is currently being discussed whether using U_{10} in the IME method, rather than U_{eff} , could actually give more robust Q estimates. For example, Thorpe et al. (2023) used U_{10} directly with their IME formulation. The main reason to avoid U_{eff} is the potential errors introduced in the quantification framework by the plume simulations required to train the $U_{\text{eff}}-U_{10}$ relationship.

Flux rate quantification with the CSF method

The CSF method was first introduced by White et al. (1976), in an application case related to pollutant emissions, and was first used for satellite-based methane emission quantification by Varon et al. (2018). The CSF method consists of associating the emission rate to the product of methane enhancement and wind speed integrated over the across-direction of the plume elongated axis (cross sections).

The source rate is inferred from the product of the methane enhancement and the wind speed integrated across the plume width. Using the formulation in Pandey et al. (2023), this can be expressed as

$$Q = C \cdot U_{\text{eff}} \quad (3.6)$$

where

$$C = \frac{1}{n} \sum_{j=1}^n \int \hat{\alpha}(x_j, y) dy. \quad (3.7)$$

The y -direction is the direction perpendicular to the wind, and the calculation is averaged over transects at different downwind positions (x_j) in order to obtain a more robust Q estimate.

One advantage of the CSF method with respect to the IME method is that the CSF method can be used for plumes which are not completely contained in the imaged area. On the other hand, the dependence on wind direction is an additional source of error relative to the IME method (Jacob et al., 2022).

3.3 Machine learning-based methods for plume detection and quantification

There is a rapid evolution in the use of machine-learning methods for the automatic detection and/or quantification of methane plumes in high spatial resolution satellite data. Deep learning models in particular manage to model the characteristics of methane plumes and to efficiently distinguish them from the background and spectral confusers. These developments have been motivated by the need for scalable methods to reach global scale and live monitoring of methane emissions. Indeed, machine learning models largely alleviate the need for manual expert labeling, even though none of the published methods have managed yet to reach the level of accuracy achieved by human experts. Consequently, the detections of the models still need to be validated by a human expert, but this is insignificant compared to a fully manual approach. Another challenge lies in the lack of exhaustive open-source datasets to compare models' performance and validate results effectively.

Some of these machine learning models also produce the quantification by estimating the emission rate of the plume detected solely based on the satellite images. This introduces a level of independence from external wind source data, which often lack precision and are available at a very coarse spatial resolution, but this comes at the cost of black box uncertainties whose dependence to the input parameters is hard to identify.

To sum up, the use of machine learning models for methane emissions monitoring need to satisfy a trade-off between scalability and timeliness, versus precision and explainability.

We list some examples in this section:

Růžička et al. (2023):

The machine learning-based models HyperSTARCOP and MultiSTARCOP were developed for the semantic segmentation of methane plumes in hyperspectral and multispectral data, respectively. In order to train the models, a dataset of hyperspectral images from the AVIRIS-NG instrument was compiled, which allowed the simulation of multispectral acquisitions of the same data. The HyperSTARCOP model shows a better performance than a state-of-the-art matched

filter-based approach (Foote et al., 2020) with an increase by over 25% in the F1 score and a reduction in the fraction of false positives by over 42%. Moreover, the model shows a zero-shot generalization to be applied to hyperspectral data from other instruments.

Joyce et al. (2023):

A neural network model was developed to detect and quantify methane plumes. The model training was carried out by using synthetic images that combined PRISMA data and simulated plumes obtained from large eddy simulations. A F1 score of 0.95 and a mean error of 24% were obtained for the plume detection and the quantification, respectively, although a larger training dataset is expected to improve these results. The rapid processing of this model for the detection and quantification of methane plumes is shown as an advantage to reduce the time and costs to tackle climate change.

Vaughan et al. (2024):

The deep learning model CH4Net allows for the monitoring of methane plumes from super-emitters using Sentinel-2 data. This model is the first to offer fully automated monitoring of super-emitter sites, and it created the pioneering large-scale dataset of methane plumes detected in Sentinel-2 images. Although the model only need one single pass (one acquisition), it significantly outperforms the methane emission detection based on the multi-band multi-pass (several acquisitions) state-of-the-art approach by over 60% in semi-arid areas, although the false positive rate remains similar.

Jongaramrungruang et al. (2022):

The convolutional neural network model MethaNet was developed to automatically quantify methane plumes detected in retrievals obtained from AVIRIS-NG data. This model has been trained by means of large eddy simulations of methane plumes adapted to typical noise values of different scenarios. As a result, it estimates plume flux rate values without using ancillary wind data and performs a mean absolute percentage error of about 17%, which significantly improves the precision over previous methods that needed wind speed information.

Bruno et al. (2024):

The machine learning-based algorithm U-Plume was designed for the automated detection and quantification of methane plumes, although it can also be applied to CO₂ using a proper training dataset. This model was tested in GHGSat-C1 data including scenes with different levels of heterogeneity, where simulated methane plumes from large eddy simulations were integrated. The detection and delineation of plumes with flux rate values as low as 100 kg/h were possible under favorable conditions applying the U-Plume model. Moreover, the wind speed and the plume delineations were the main error sources in the quantification at low and high wind speed values, respectively. In addition, a new metric called the point-source observability was defined as a combination of those parameters that have more impact on detection and masking, resulting in a successful parameter to predict the detection and quantification of point-source emissions.

3.4 Validation of emission rate estimates and plume detection limits

The comparison of satellite-based Q estimates with ground-based controlled-releases of methane is the main approach for the validation of Q estimates and the evaluation of detection limits.

Two major controlled-release experiments were carried out in 2021 and 2022 by Adam Brandt's group at Stanford University. These tests enabled single-blind testing of flux rate estimates from a number of high resolution satellites. The two tests differed in the satellites involved, the location, and the range of released methane volumes. The first campaign took place at desert site in Ehrenberg, Arizona (USA), over a 19-day period from 16 October to 3 November, 2021 (Sherwin et al., 2023). The metered flux rates ranged from 0.2 to 7.2 metric tons per hour (t/h). Five satellites were tested (GHGSat-C2, PRISMA, Sentinel-2, Landsat 8, and WorldView-3). A total of 19 match-ups between satellite-based and metered flux rates was obtained. In the second campaign, taking place in Arizona (USA), the number of satellites and validation match-ups was extended with respect to the 2021 campaign (Sherwin et al., 2024). A total of 82 controlled methane releases were conducted between 10 October and 30 November 2022 during overpasses of nine satellite constellations, which included the ones participating in the same campaign and also the EnMAP, Gaofen-5 and Ziyuan-1 hyperspectral missions. The metered flux rates ranged from 0.3 to 1.6 t/h.

Further controlled release campaigns are expected for the 2024-2026 from the same group at Stanford University, and potentially by other groups and institutions in the USA and Europe.

4 Review of methane retrieval and quantification methods for global flux mappers

Within the scope of MEDUSA, only the TROPOMI satellite instrument will currently be considered in the global flux mapper category (until launch and validated data availability of GOSAT-GW and Sentinel-5). This section first reviews different existing approaches to retrieve the methane total column from TROPOMI measurements, and then describes how emissions are quantified based on these retrievals. Figure XX shows a timeline of the flux mapper satellite instruments considered here, where GOSAT is included because of its relevance for the TROPOMI+GOSAT blended product described in Section 4.1.3.

4.1 Methane concentration retrievals

The global flux mapper TROPOMI makes measurements of near (757–774 nm) and short-wave (2305–2385 nm) infrared radiation at spectral resolutions of 0.5 and 0.25 nm, respectively, for $5.5 \times 7 \text{ km}^2$ pixels at nadir. Figure 5 provides an illustration of a TROPOMI spectrum.

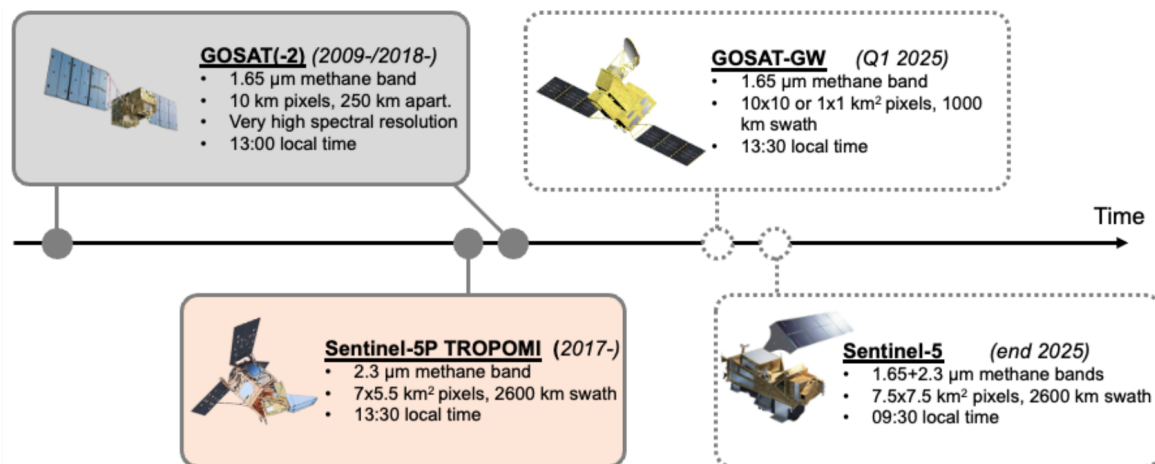


Figure 4: Flux mapper satellite instruments considered within MEDUSA. GOSAT is not able to detect point sources, but its data are used in the TROPOMI+GOSAT blended product (Section 4.1.3).

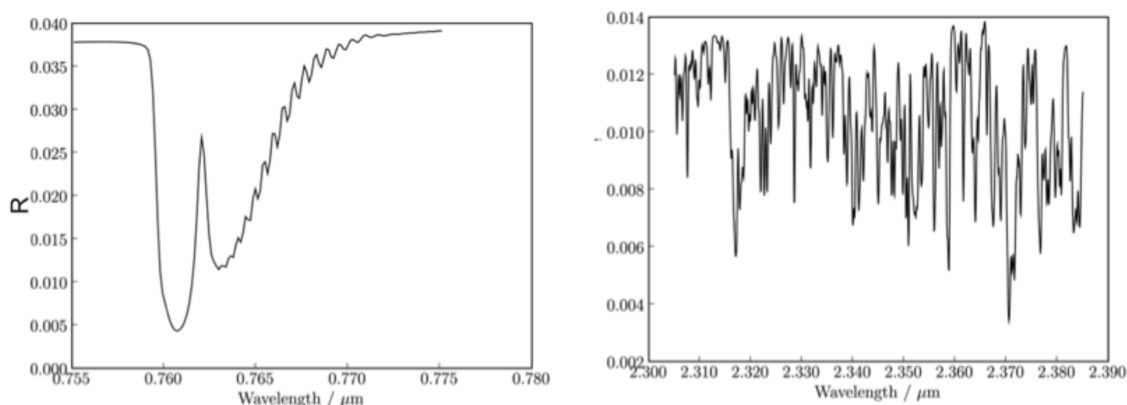


Figure 5: Example simulated spectrum at TROPOMI's spectral resolution for the near infrared (left) and shortwave infrared (right) bands. Figure taken from Hasekamp et al. (2022).

In the context of spaceborne instruments, a retrieval consists of estimating the geophysical state (of the atmosphere and of the surface) that best fits an atmospheric radiation measurement made from space. It can be formulated as:

$$\mathbf{y} = F(\mathbf{x}) + \varepsilon \quad (4.1)$$

with \mathbf{y} the measured spectrum, \mathbf{x} the state vector containing all the geophysical variables to be fitted, F , a forward radiative transfer model linking the geophysical state and the measurements made by the satellite instrument, and ε the instrument noise. Unlike multi- and hyperspectral imagers which have low spectral resolutions and samplings that do not allow to fit precise methane background columns or many other geophysical variables, the TROPOMI spectral resolution and sampling enable TROPOMI measurements to carry enough information in order to fit the

Table 2: Overview of the level-2 methane products available for Sentinel-5P TROPOMI.

Name	SRON/RemoTeC	IUP/WFM-DOAS	Blended TROPOMI+GOSAT
Spectral bands	757–774 nm, 2305–2385 nm	Two fitting windows: <ul style="list-style-type: none"> • 2311 – 2315.5 nm • 2320 – 2338 nm 	Machine Learning algorithm trained to predict TROPOMI – GOSAT bias solely based on TROPOMI retrieval results.
State vector	12-layer CH ₄ profile, CO and H ₂ O total columns, aerosol parameters, 3 rd order polynomial baseline fit, SIF, spectral shift.	Scaling factors for CO, H ₂ O, and CH ₄ profiles, T profile shift and a pressure profile scaling, 3 rd order polynomial baseline fit.	This bias is then corrected. Uses the SRON/RemoTeC data product as starting point.
Optimization method	Philips–Tikhonov regularization	Least-squares	
Filtering + a posteriori corrections	Clouds filtered from VIIRS (VIIRS-independent backup) Bias-corrected based on SAA albedo correction	Clouds filtered with RF classifier Bias-corrected by RF regressor based on CH4SLIM	
Validation against TCCON (Single measurement precision)	8.7 ppb to 19.1 ppb depending on TCCON stations	12.4 ppb	11.9 ppb
Reference	Lorente et al. (2021, 2023); ATBD ; ReadMe ; Product User Manual .	Schneising et al. (2019, 2023)	Balatus et al. (2023)

methane total column and different interfering geophysical variables, for example water vapor, carbon monoxide, albedo or aerosol-related parameters. The geophysical variables included in the state vector x , the radiative transfer model F and the estimation scheme used to solve Eq. 4.1 vary across the different groups that process TROPOMI measurements to retrieve methane total columns (denoted XCH₄). The following subsections describe existing TROPOMI methane total column products. An overview of all products is included in Table 2.

4.1.1 Operational TROPOMI XCH₄ product, RemoTeC/SRON

The operational TROPOMI XCH₄ product is based on the SRON-developed RemoTeC inverse scheme which has been demonstrated on other satellite instruments besides TROPOMI, such as GOSAT (Butz et al., 2011), and OCO-2 (Wu et al., 2018). It uses the LINTRAN V2.0 radiative transfer model (Schepers et al., 2014; Landgraf et al., 2001) to simulate TROPOMI measurements, including aerosol scattering effects, and the Philips–Tikhonov regularization scheme to solve the retrieval inverse problem. Both relevant TROPOMI bands are taken into account in

the measurement vector (757–774 nm and 2305–2385 nm, see Fig. 5). The state vector contains methane partial sub-column number densities in 12 equidistant pressure layers, total columns of carbon monoxide and water vapor, and aerosol- and albedo-related (third-order polynomial) parameters. Sun-induced fluorescence and spectral shift are also fitted from the near infrared band.

Clouds are filtered relying on observations by the Visible Infrared Imaging Radiometer Suite (VIIRS) instrument flying a few minutes ahead of TROPOMI, pixel quality is evaluated based on retrieval-relevant metrics. A backup cloud filter only using TROPOMI data that uses a machine learning approach trained on historic VIIRS data has been operational since Fall 2023 (Borsdorff et al., 2024). Raw XCH₄ results are corrected a posteriori to remove albedo-dependent biases evaluated with the “small area approximation”, which assumes that retrieved values should be uniformly distributed against albedo over small regions (O’Dell et al., 2018; Lorente et al., 2021).

Compared to reference XCH₄ data from Total Carbon Column Observing Network (TCCON) (Wunch et al., 2011), the bias-corrected XCH₄ results from the operational TROPOMI product show a mean bias of -5.3 ppb and a station-to-station variability of 5.1 ppb (Lorente et al., 2023). Station-wise single measurement precisions (or standard deviations of the difference between TCCON and TROPOMI operational XCH₄) range from 8.7 ppb to 19.1 ppb.

A comprehensive detailed description of the operational TROPOMI XCH₄ product is provided by Hasekamp et al. (2022) and Lorente et al. (2021, 2023).

4.1.2 WFMD/Bremen

The WFM-DOAS (WFMD) retrieval algorithm (Buchwitz et al., 2000) has been developed at the University of Bremen and has previously been demonstrated on the SCIAMACHY satellite missions (e.g. Buchwitz et al., 2005, 2006). It relies on pre-computed radiances (and their partial derivatives) simulated with the SCIATRAN radiative transfer model (Rozanov et al., 2002, 2014) and uses a least-squares estimation scheme to solve the retrieval inverse problem. The measurement vector includes two fitting windows (2311–2315.5 and 2320–2338 nm) comprised within the shortwave infrared band measured by TROPOMI. The state vector contains scaling factors for carbon monoxide, water, and methane profiles, temperature profile shift and a scaling of the pressure profile, along with a third-order polynomial baseline fitting.

Cloudy and low-quality scenes are filtered based on the retrieval output using a random-forest classifier trained against VIIRS-based labels. Subsequently, raw XCH₄ results are calibrated using a random forest regressor trained against the Simple climatological Model for atmospheric CH₄ (SLIMCH₄) v2021, which satisfactorily compares to TCCON reference columns.

Compared to reference XCH₄ data from TCCON, the WFMD/TROPOMI product shows a mean bias of 5.2 ppb and a single measurement precision of 12.4 ppb.

A comprehensive description of WFMD/TROPOMI is provided by Schneising et al. (2019)

and the latest developments are presented by Schneising et al. (2023).

4.1.3 Blended TROPOMI+GOSAT satellite data product

The TROPOMI satellite instrument has daily global coverage but does not benefit from a spectral resolution as high as GOSAT's, which coverage is however very sparse. GOSAT also has an additional 1.6 μm channel thereby allowing the use of the proxy approach. An initial version of the TROPOMI operational algorithm suffered from larger retrieval biases caused by the mis-interpretation of (correlated) interfering geophysical variables (e.g., clouds, aerosols, albedo, etc.) compared to GOSAT. Relying on an ensemble of TROPOMI and GOSAT co-located measurements, Balasus et al. (2023) developed a machine learning model trained to predict and correct the TROPOMI – GOSAT bias in TROPOMI data using only variables included in TROPOMI retrieval files. The largest corrections performed by this model are associated with coarse aerosol particles and high shortwave infrared albedo.

Compared to reference methane XCH₄ data from TCCON, the blended TROPOMI+GOSAT product shows a mean bias of 4.4 ppb and a single measurement precision of 11.9 ppb.

A comprehensive description of the blended TROPOMI+GOSAT product is provided by Balasus et al. (2023).

4.2 Emission detection and quantification methods

The focus of MEDUSA will be detecting and quantifying individual plumes. Thus, this section first reviews plume-based methods, from detection to quantification of the associated emission rate. Beyond plume-based methods, observations from several overpasses can be used together to estimate emissions, these approaches are presented in the second part of this section.

4.2.1 Plume detection methods for a known source

When a target source is defined, detecting a plume boils down to identifying enhanced pixels downwind of the source. In addition to statistical analysis of the pixels surrounding the target source to identify enhanced XCH₄ values, the wind direction can be exploited to refine the selection. For example, Sadavarte et al. (2021) use an elongated box downwind of the source location that iteratively explores different directions around the wind direction, and then different box lengths along the selected direction to find an emission plume.

4.2.2 Automatic plume detection by machine learning

Data-driven machine learning methods are efficient approaches to detect plumes without prior knowledge of source location. Two main automated plume detection products using TROPOMI XCH₄ data are currently available (Lauvaux et al., 2022; Schuit et al., 2023).

Lauvaux et al. (2022) present a two-step approach, based on the computation of a TROPOMI methane anomaly map applied to the L2 data V02.05.00. Continuous groups of positive pixels in the anomaly map are selected as plume candidates, and contiguous (but distinct) plumes are separated using watershed segmentation. The detections are systematically validated by two human expert labelers who filter out false positives. They do this by verifying the presence of a potential emission source and assessing the consistency of the detection based on geometric features, wind alignment, and albedo.

Schuit et al. (2023) uses a 2-step machine learning procedure to automatically detect plumes in TROPOMI data. First, each TROPOMI orbit image is swept by a 32×32 pixel moving window approach with 50% overlap in both across- and along-track directions. Every 32×32 pixel image is first analyzed by a Convolutional Neural Network (CNN) determining if the image contains a plume-like signal in the methane field. If positive, the image is subsequently examined by a Support Vector Classifier (SVC) that further analyzes the detection for possible artefacts (e.g. due to albedo features). In case of detection confirmed by the SVC, the Class Activation Map (CAM) of the CNN is multiplied by the methane enhancement values (calculated by subtracting a local background) contained in the 32×32 pixel image to identify the pixel with the highest enhancement and confidence as belonging to the plume. Starting from this pixel, a plume mask is generated using an iterative outward dilation approach, including pixels with enhancements 1.8 standard deviations or more above the image mean in the plume mask. The plume mask is final once the pixel selection converges, and is used to calculate the methane emission rate associated with this plume. At this stage, similarly to Lauvaux et al. (2022), plumes are also manually verified by two human expert labelers to clear detections from potentially remaining artefacts. An overview of plumes detected using this approach for 2021 is included in Fig. 6.

4.2.3 Plume-based quantification methods

Quantification methods for individual plumes range from mass balance methods, which do not require the use of atmospheric transport models, such as the Integrated Mass Enhancement (IME) method and Cross-Sectional Flux (CSF) method, to full inversions using atmospheric transport models.

The IME and CSF methods for TROPOMI

A description of the IME and CSF mass-balance methods for the quantification of methane plumes from high-resolution satellite data is already provided in Section 3.2. The formulation of

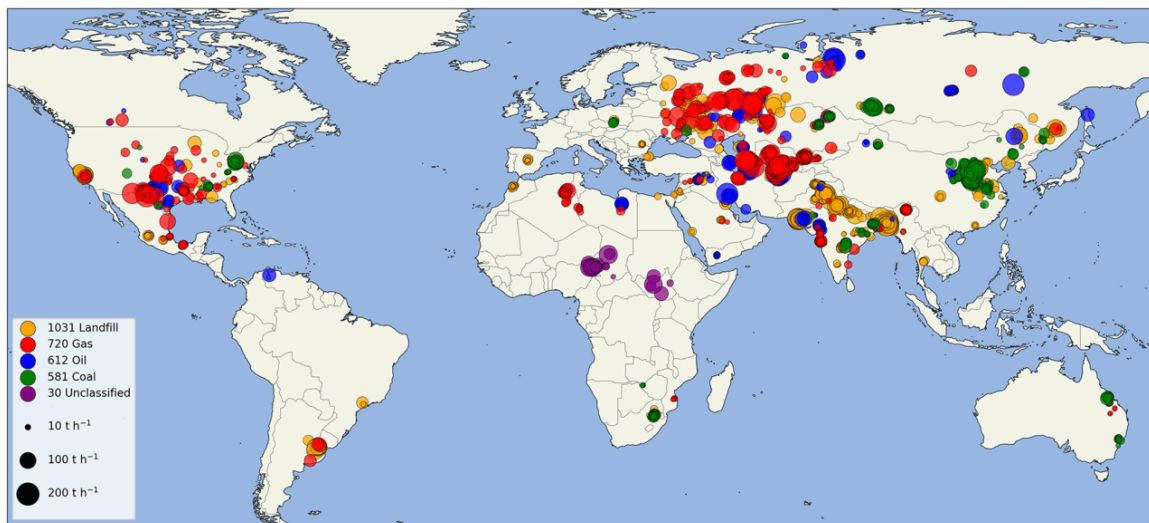


Figure 6: Overview of 2021 TROPOMI methane plumes detected in Schuit et al. (2023). Source sectors estimates are based on bottom-up emission inventories. [From Schuit et al. (2023)]

these methods is similar for TROPOMI despite the very different retrieval sensitivity and spatial resolution.

In particular, the $U_{\text{eff}} = 0.47 \cdot U_{\text{PBL}} + 0.31$ and $U_{\text{eff}} = 0.59 \cdot U_{10}$ relationships have been used for the IME model with TROPOMI by Schuit et al. (2023), with U_{PBL} being the wind speed averaged over the Planetary Boundary Layer thickness, whereas $U_{\text{eff}} = (1.05 \pm 0.17)U_{\text{PBL}}$ was derived for TROPOMI's resolution by Varon et al. (2019). This method has for example been used for TROPOMI plume quantifications with the CSF model by Sadavarte et al. (2021).

Atmospheric inversion for plumes observed in a single overpass

Atmospheric inversion (e.g. Ciaïis et al., 2010) leverages forward atmospheric transport modelling combined with an inversion approach to obtain the fluxes that best fit a set of atmospheric observations (TROPOMI XCH₄ here). Different strategies of variable complexity can be employed to combine the information brought by atmospheric simulation on one side, and satellite data on the other.

An enhancement scaling approach is the simplest application of a modeled plume to quantify emissions of an observed plume. For example, it has been used to quantify the emissions of a well blowout by Pandey et al. (2019). In Lauvaux et al. (2022), each detection is quantified using a corresponding simulated plume, calculated with the Lagrangian particle dispersion model HYSPLIT (Stein et al., 2015). The simulation is conducted in forward mode on a 0.01×0.01 -degree grid, using meteorological data from the Global Forecast System (GFS) provided by the National Centers for Environmental Prediction (NCEP). The emission rate is finally obtained by normalizing the flow rate of the simulated plume with the ratio of enhancement between the actual observation and the simulation. Examples for TROPOMI-detected and simulated plumes

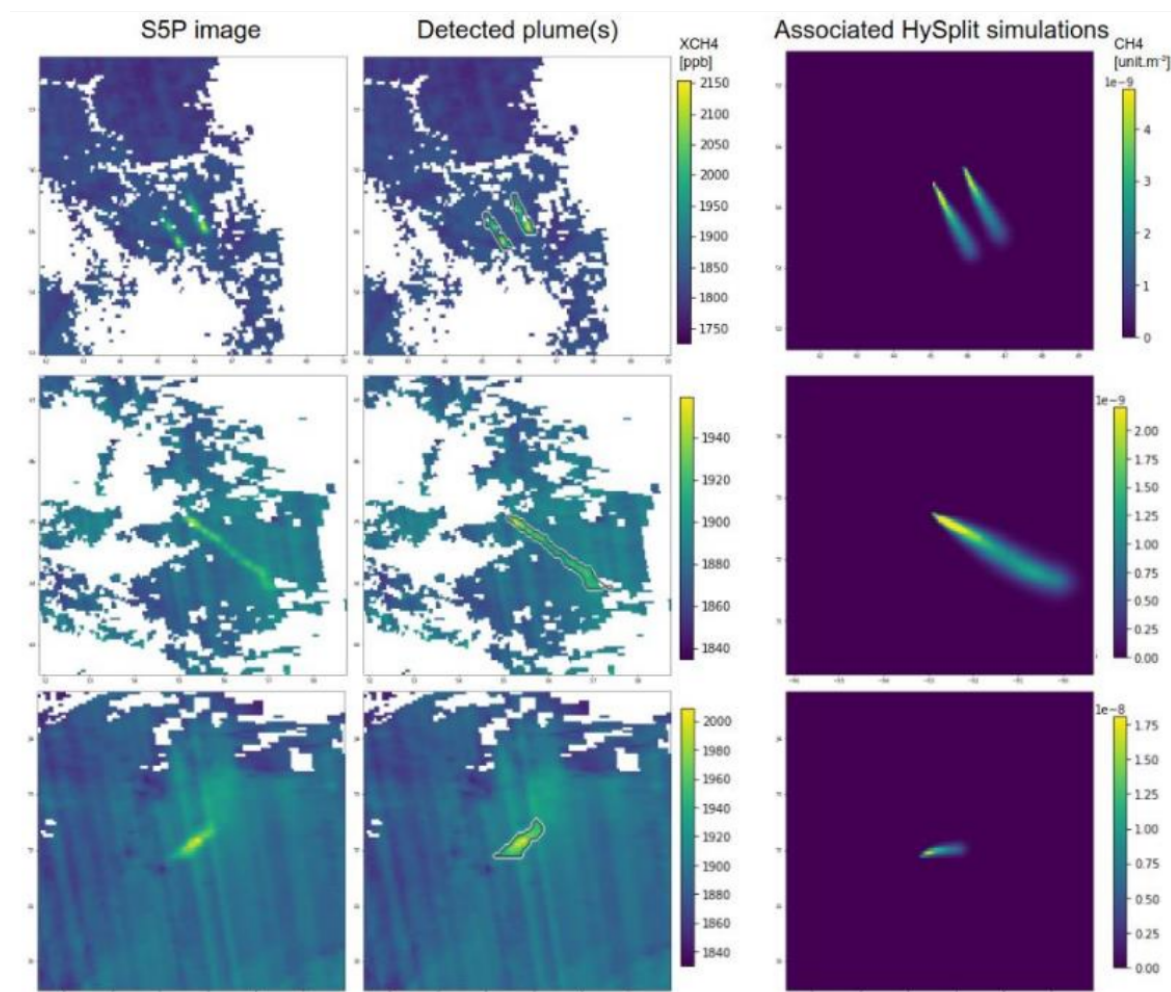


Figure 7: Examples of TROPOMI methane images (Left), TROPOMI-detected methane plumes (Center), and HySplit-simulated plumes used to quantify the TROPOMI-detected plumes (Right). [From Lauvaux et al. (2022)]

are shown in Fig. 7.

Estimation schemes, such as the framework brought by Optimal Estimation Inversion (Rodgers, 2000), can also be employed to quantify individual plumes. For example, Maasackers et al. (2022a) and Guanter et al. (2024) use analytical Bayesian inversions with the Weather Research & Forecasting Model (WRF) model to quantify TROPOMI plumes originating from large blowout events.

4.2.4 Methods relying on multiple TROPOMI overpasses

Besides plume-based emission quantification that rely on single TROPOMI overpasses, other methods have been developed or can be applied to detect and quantify emissions from TROPOMI XCH4 observations obtained over several overpasses. This subsection presents some of them.

Persistent emitter detection and mass balance quantification

Vanselow et al. (2024) developed a method to detect and quantify persistent methane emitters using monthly gridded global averages (0.1×0.1 degree resolution) of the WFMD/TROPOMI XCH₄ product. For 2018–2021, they analyze monthly gridded averages in the following manner:

- Pixel filtering based on the number of available overpasses and elevation corrections are performed on monthly global gridded TROPOMI methane maps.
- Background methane concentration is estimated and removed from the monthly global gridded maps based on a set of five high pass filters of sizes ranging from 1×1 to 5×5 degree, yielding five different monthly gridded global anomaly maps.
- For each high pass filter size, the methane anomalies are examined in the temporal dimension to identify persistent potential source regions. Region masks are refined using the multi-year 2018-2021 gridded average and potential artefacts caused by inhomogeneous albedo or complicated topography are removed. Finally, results for all five high pass filter sizes are combined.

Methane emissions of persistent potential source regions are subsequently quantified using the fast data-driven quantification approach first presented by Buchwitz et al. (2017) for uniformly ventilated area sources. We have:

$$Q = \delta XCH_4 \times M \times M_{eq} \times L \times V \times 2 \quad (4.2)$$

with Q the emission rate, δXCH_4 the XCH₄ enhancement over the persistent potential source region, L the effective source length defined as the square root of the region area, V the averaged wind speed over the region and $M \times M_{eq}$ factors to convert column enhancement into mass change per area. The uncertainty is evaluated accounting for uncertainties in the methane enhancements and wind speed. An example application for the Permian Basin is included in Fig. 8.

Divergence method

The divergence method is a computationally-light approach to obtain emission maps. It associates emissions for a given point in space with the divergence of advective fluxes. We have:

$$Q = \nabla \cdot \mathbf{F}^{adv} \quad (4.3)$$

with Q the emission rate, ∇ the divergence operator and $\mathbf{F}^{adv} = C\mathbf{V}$ the advective flux of methane, with \mathbf{V} the wind vector and C the methane column.

This approach was pioneered by Beirle et al. (2019) for TROPOMI NO₂ observations, and then applied to TROPOMI XCH₄ by, for example, Liu et al. (2021) and Veeffkind et al. (2023).

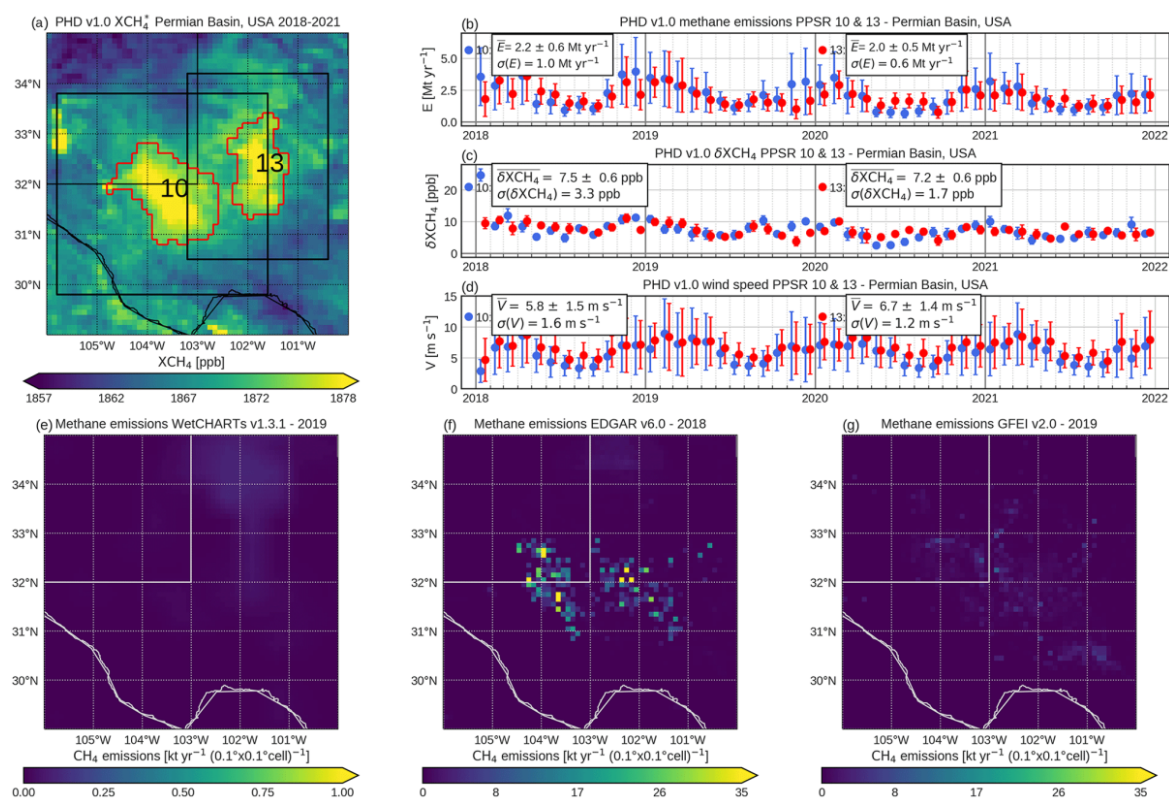


Figure 8: Example of the Vanselow algorithm applied to the Permian basin showing: (a) TROPOMI concentrations with delineated hot spot regions, (b) time series of quantifications based on (c) enhancements and (d) wind speed, and (e-g) comparisons to bottom-up inventories. [From Vanselow et al. (2024)]

Important methodological aspects related to turbulent diffusion are discussed by Roberts et al. (2023) and related to vertical wind profiles, temporal averaging and non-zero methane backgrounds by Koene et al. (2024).

The wind-assigned anomaly method

This method was first presented by Tu et al. (2022a) and applied to estimate methane emissions of the Madrid city area. It consists of creating two average concentration maps of TROPOMI XCH_4 enhancement for a target region: one map averaging days when the wind blows along its principal direction (considering local climatology), and one map averaging days when the wind blows in other directions. The difference between these two maps yields a wind-assigned methane anomaly map showing positive enhancements downwind from the target region, and negative ones upwind (considering the principal wind directions). This wind-assigned anomaly map is compared to a synthetic one, obtained by simulating all sources within the target region with simple plume models (Gaussian or cone plumes), and the simulated emission rates are scaled so that the modelled wind-assigned anomaly fits the observed one. Uncertainty estimates are obtained perturbing various input parameters. This method has been applied to estimate urban emissions from the Madrid city area (Tu et al., 2022a), coal mine emissions in

Poland (Tu et al., 2022b) and in Shanxi, China (Tu et al., 2024).

Atmospheric inversions using multiple overpasses

Atmospheric inversions using optimal estimation schemes presented earlier (see dedicated paragraph in Section 4.2.3 “Plume-based quantification methods”) can accommodate single- as well as multi-overpass satellite observations. For example, Zhang et al. (2020) and (Schneising et al., 2020) used TROPOMI data to estimate methane emissions from the Permian and Maasakkers et al. (2022b) employed an atmospheric inversion to estimate yearly methane emissions from four major cities.

5 Review of available online methane data portals

The following online data portals provide satellite-based information on anthropogenic methane emissions:

- IMEO Methane Data Portal: Collection of methane plumes detected from a number of satellites, mostly from point sources analysed by IMEO’s Methane Alert and Response System (see screenshot in Fig. 9). Data access is free.
- EMIT Open Data Portal: Collection of methane plumes detected from EMIT data by data analysts at NASA JPL. Data access is free.
- SRON Methane Plume Maps: Weekly lists of large methane plumes detected from TROPOMI by the SRON team. Data access is free.
- GHGSat’s SPECTRA portal: Data visualization and analysis platform based on methane data from GHGSat and third-party satellites. Requires registration.
- Kayrros Methane Watch: Data platform developed by Kayrros for near real-time monitoring of methane hotspots based on methane data from TROPOMI and other publicly-available methane-sensitive satellites. Requires registration.

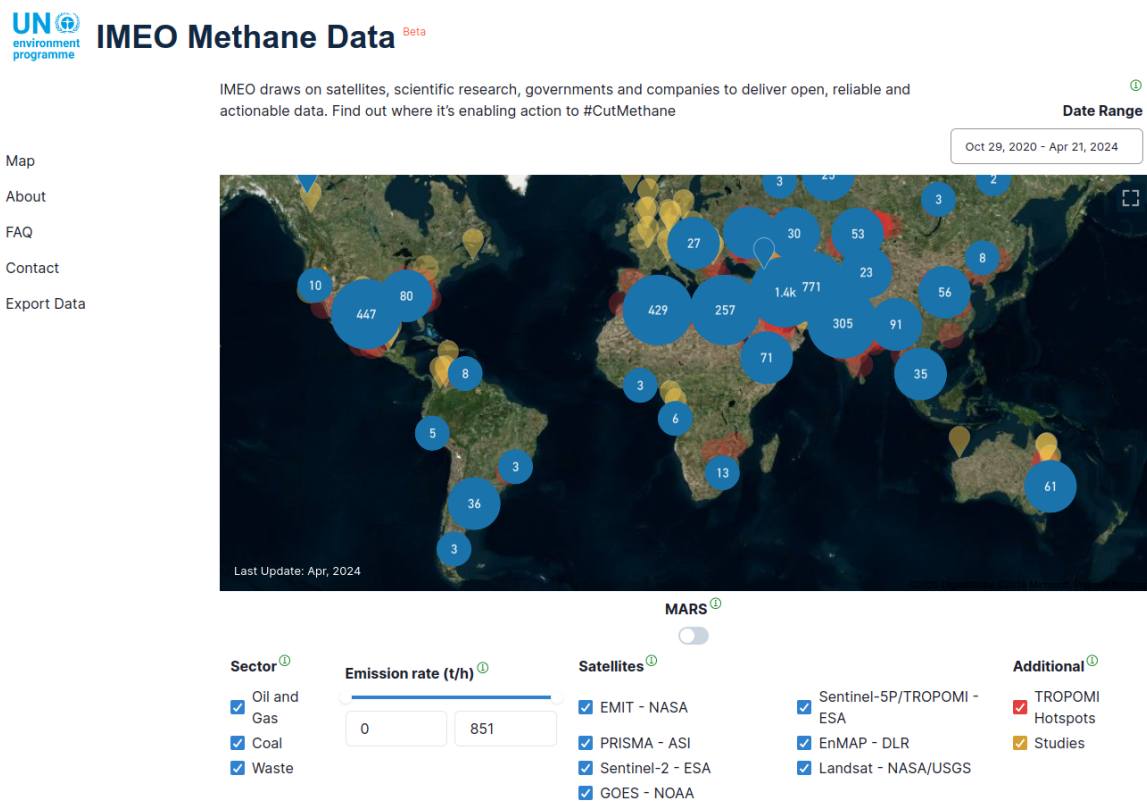


Figure 9: Screenshot of the IMEO Methane Data Portal.

6 Review of methane-related activities of relevance to MEDUSA

The following recent and ongoing projects deal with satellite remote sensing of anthropogenic methane sources:

- **ESA SMART-CH4 (Satellite Monitoring of Atmospheric Methane):** it is part of the EC-ESA JOINT EARTH SYSTEM SCIENCE INITIATIVE. It builds upon previous experience and projects in satellite-based methane quantification, aiming to enhance emission products derived from satellites. The key objectives and tasks of SMART-CH4 include the enhancement of TROPOMI retrievals and multi-sensor products, the utilisation of improved products to deepen our understanding of regional methane budgets, and the attribution of recent trends in CH4 concentrations.
- **EU EYE-CLIMA:** it aims to improve estimates of emissions and removals of the most important greenhouse gases, as well as black carbon, to support European and international policy to reduce emissions. It includes tasks focusing on satellite methane retrievals including emission estimates.
- **ESA's GHG-CCI+ project of ESA's Climate Change Initiative (CCI):** The objective of

the GHG-CCI+ project is to further develop retrieval algorithms needed to generate new high quality satellite-derived CO₂ and CH₄ atmospheric data products. The project team consists of leading European experts on satellite methane and CO₂ retrieval, validation and user assessments in terms of methane and CO₂ inverse modelling.

- **ESA High resolution methane mapping with hyper and multispectral data (HiResCH₄):** it was funded by ESA's Future EO-1 Open Call for Proposals and led by the LARS group at the UPV. HiResCH₄ (2021-2024) initially focused on the development of new methods for the detection and quantification of methane plumes with the PRISMA, Sentinel-2, Landsat, and Worldview-3 high spatial resolution hyperspectral and multispectral instruments, and was extended in 2023 in order to cover methane retrievals from the EnMAP mission, the Sentinel-2 NG future mission, and offshore methane retrievals.
- **Kayrros' Methane Watch:** world's first operational system for near real-time monitoring of substantial methane hotspots, developed and operated by Kayrros. It includes methane plume detections along with quantifications for more than 10 different constellations. An open-source version with a limited content is available.
- **IMEO MARS:** the Methane Alert and Response System (MARS) of UNEP's International Methane Emissions Observatory (IMEO) is the first global satellite detection and notification system providing actionable data on very large methane emissions around the world. Its goal is to accelerate implementation of the Global Methane Pledge by transparently scaling up global efforts to detect and act on major methane emissions sources
- **IMEO Methane Science Studies:** IMEO methane science studies help understand global methane emissions thanks to a series of scientific studies led by academics and scientists, often relying on remote sensing data. The current focus is on the oil, gas, and coal sectors.
- **EUMETSAT MTG-FCI Methane Detection Activity (FCI-CH₄):** it is funded by EUMETSAT and performed by the UPV-LARS group between 2023 and 2024. It deals with the detection of methane super-emissions with the Flexible Combined Imager onboard the Meteosat Third Generation geostationary platform.
- **Controlled-release tests led by Stanford University and METEC:** ongoing series of controlled methane releases intended for the validation of plume detections and flux rate estimates by a number of satellites.
- **EMIT methane plume intercomparison project:** led by the U.S. National Institute of Standards and Technology (NIST), this project is coordinating the intercomparison of algorithms for the detection and quantification of methane plumes with EMIT.
- **AI4CH₄:** Starting in early 2025, AI4CH₄ will utilise AI and machine learning to detect methane point sources from satellite imagery, enhancing the ability to monitor and quantify methane emissions.

- **IM4CA – Investigating Methane for Climate Action:** IM4CA is a 4-year project that will start in January 2025 on “Enhanced quantification and understanding of natural and anthropogenic methane emissions and sinks”. The project brings together 26 partners from 14 countries and is coordinated by the VU Amsterdam. The objective of the project is to reduce emission uncertainties through enhanced atmospheric monitoring, covering both additional measurements and improved modeling. Measurement campaigns will include coverage of Romania and tropical Africa. Furthermore, focus will be on improving emission inventories including of natural emissions, incorporation of multiple observations including satellites into inverse analyses, and recommendations for climate actions on methane emissions.
- **CAMS Methane project:** Since May 2024, SRON is providing a CAMS service on ‘Development and provision of hot-spot observation-based emissions of methane’ with sub-contractors MPI-Meteorology Hamburg and IUP- University Bremen. The service provides satellite-based detections of methane plumes from emission hot spots using Sentinel-5P TROPOMI data on at least weekly basis, building on the methodology from Schuit et al. (2023). Furthermore, these detections are routinely compared to hot spot detections and quantifications coming from the Integrated Forecasting System (IFS). Finally, comprehensive expert (user) support on the service is provided.
- **ESA’s World Emission project:** it integrates satellite data and models to provide global emissions estimates for various trace gases, including methane, through an advanced on-line system. This platform not only facilitates visualization and analysis but also enables real-time tracking of emission sources and trends.

7 References

- Balagus, N., Jacob, D. J., Lorente, A., Maasackers, J. D., Parker, R. J., Boesch, H., Chen, Z., Kelp, M. M., Nesser, H., Varon, D. J., 2023. A blended tropomi+gosat satellite data product for atmospheric methane using machine learning to correct retrieval biases. *Atmospheric Measurement Techniques* 16 (16), 3787–3807.
URL <https://amt.copernicus.org/articles/16/3787/2023/>
- Beirle, S., Borger, C., Dörner, S., Li, A., Hu, Z., Liu, F., Wang, Y., Wagner, T., 2019. Pinpointing nitrogen oxide emissions from space. *Science Advances* 5 (11), eaax9800.
URL <https://www.science.org/doi/abs/10.1126/sciadv.aax9800>
- Berk, A., Conforti, P., Kennett, R., Perkins, T., Hawes, F., van den Bosch, J., 2014. Modtran@ 6: A major upgrade of the modtran@ radiative transfer code. In: 2014 6th Workshop on Hyperspectral Image and Signal Processing: Evolution in Remote Sensing (WHISPERS). pp. 1–4.
- Borchardt, J., Gerilowski, K., Krautwurst, S., Bovensmann, H., Thorpe, A. K., Thompson, D. R., Frankenberg, C., Miller, C. E., Duren, R. M., Burrows, J. P., 2021. Detection and quantification of ch₄ plumes using the wfm-doas retrieval on aviris-ng hyperspectral data. *Atmospheric Measurement Techniques* 14 (2), 1267–1291.
URL <https://amt.copernicus.org/articles/14/1267/2021/>
- Borsdorff, T., Martinez-Velarte, M. C., Sneep, M., ter Linden, M., Landgraf, J., 2024. Random forest classifier for cloud clearing of the operational tropomi xch₄ product. *Remote Sensing* 16 (7).
URL <https://www.mdpi.com/2072-4292/16/7/1208>
- Bruno, J. H., Jervis, D., Varon, D. J., Jacob, D. J., 2024. U-plume: automated algorithm for plume detection and source quantification by satellite point-source imagers. *Atmospheric Measurement Techniques* 17 (9), 2625–2636.
URL <https://amt.copernicus.org/articles/17/2625/2024/>
- Buchwitz, M., de Beek, R., Burrows, J. P., Bovensmann, H., Warneke, T., Notholt, J., Meirink, J. F., Goede, A. P. H., Bergamaschi, P., Körner, S., Heimann, M., Schulz, A., 2005. Atmospheric methane and carbon dioxide from sciamachy satellite data: initial comparison with chemistry and transport models. *Atmospheric Chemistry and Physics* 5 (4), 941–962.
URL <https://www.atmos-chem-phys.net/5/941/2005/>
- Buchwitz, M., de Beek, R., Noël, S., Burrows, J. P., Bovensmann, H., Schneising, O., Khlystova, I., Bruns, M., Bremer, H., Bergamaschi, P., Körner, S., Heimann, M., 2006. Atmospheric carbon

- gases retrieved from sciamachy by wfm-doas: version 0.5 co and ch₄ and impact of calibration improvements on co₂ retrieval. *Atmospheric Chemistry and Physics* 6 (9), 2727–2751.
URL <https://acp.copernicus.org/articles/6/2727/2006/>
- Buchwitz, M., Rozanov, V. V., Burrows, J. P., 2000. A near-infrared optimized doas method for the fast global retrieval of atmospheric ch₄, co, co₂, h₂o, and n₂o total column amounts from sciamachy envisat-1 nadir radiances. *Journal of Geophysical Research: Atmospheres* 105 (D12), 15231–15245.
URL <https://agupubs.onlinelibrary.wiley.com/doi/abs/10.1029/2000JD900191>
- Buchwitz, M., Schneising, O., Reuter, M., Heymann, J., Krautwurst, S., Bovensmann, H., Burrows, J. P., Boesch, H., Parker, R. J., Somkuti, P., Detmers, R. G., Hasekamp, O. P., Aben, I., Butz, A., Frankenberg, C., Turner, A. J., 2017. Satellite-derived methane hotspot emission estimates using a fast data-driven method. *Atmospheric Chemistry and Physics* 17 (9), 5751–5774.
URL <https://acp.copernicus.org/articles/17/5751/2017/>
- Butz, A., Guerlet, S., Hasekamp, O., Schepers, D., Galli, A., Aben, I., Frankenberg, C., Hartmann, J.-M., Tran, H., Kuze, A., Keppel-Aleks, G., Toon, G., Wunch, D., Wennberg, P., Deutscher, N., Griffith, D., Macatangay, R., Messerschmidt, J., Notholt, J., Warneke, T., 2011. Toward accurate co₂ and ch₄ observations from gosat. *Geophysical Research Letters* 38 (14).
URL <https://agupubs.onlinelibrary.wiley.com/doi/abs/10.1029/2011GL047888>
- Carbon Mapper Inc., 2021. Carbon Mapper. <https://carbonmapper.org/>.
- Ciais, P., Rayner, P., Chevallier, F., Bousquet, P., Logan, M., Peylin, P., Ramonet, M., Nov 2010. Atmospheric inversions for estimating co₂ fluxes: methods and perspectives. *Climatic Change* 103 (1), 69–92.
URL <https://doi.org/10.1007/s10584-010-9909-3>
- Cusworth, D. H., Duren, R. M., Thorpe, A. K., Pandey, S., Maasackers, J. D., Aben, I., Jervis, D., Varon, D. J., Jacob, D. J., Randles, C. A., Gautam, R., Omara, M., Schade, G. W., Dennison, P. E., Frankenberg, C., Gordon, D., Lopinto, E., Miller, C. E., 2021. Multisatellite imaging of a gas well blowout enables quantification of total methane emissions. *Geophysical Research Letters* 48 (2), e2020GL090864, e2020GL090864 2020GL090864.
URL <https://agupubs.onlinelibrary.wiley.com/doi/abs/10.1029/2020GL090864>
- de Jong, T. A., Maasackers, J. D., Irakulis-Loitxate, I., Randles, C. A., Tol, P., Aben, I., 2024. Daily global methane super-emitter detection and source identification with sub-daily tracking. *EarthArXiv eprints*.
- Environmental Defense Fund, 2021. MethaneSAT. <https://www.methanesat.org/>.
-

- Foote, M. D., Dennison, P. E., Thorpe, A. K., Thompson, D. R., Jongaramrungruang, S., Frankenberg, C., Joshi, S. C., 2020. Fast and accurate retrieval of methane concentration from imaging spectrometer data using sparsity prior. *IEEE Transactions on Geoscience and Remote Sensing* 58 (9), 6480–6492.
- Frankenberg, C., Thorpe, A. K., Thompson, D. R., Hulley, G., Kort, E. A., Vance, N., Borchardt, J., Krings, T., Gerilowski, K., Sweeney, C., Conley, S., Bue, B. D., Aubrey, A. D., Hook, S., Green, R. O., 2016. Airborne methane remote measurements reveal heavy-tail flux distribution in four corners region. *Proceedings of the National Academy of Sciences* 113 (35), 9734–9739.
URL <https://www.pnas.org/content/113/35/9734>
- Gorroño, J., Varon, D. J., Irakulis-Loitxate, I., Guanter, L., 2023. Understanding the potential of Sentinel-2 for monitoring methane point emissions. *Atmospheric Measurement Techniques* 16 (1), 89–107.
- Guanter, L., Irakulis-Loitxate, I., Gorroño, J., Sánchez-García, E., Cusworth, D. H., Varon, D. J., Cogliati, S., Colombo, R., 2021. Mapping methane point emissions with the prisma spaceborne imaging spectrometer. *Remote Sensing of Environment* 265, 112671.
URL <https://www.sciencedirect.com/science/article/pii/S0034425721003916>
- Guanter, L., Roger, J., Sharma, S., Valverde, A., Irakulis-Loitxate, I., Gorroño, J., Zhang, X., Schuit, B. J., Maasackers, J. D., Aben, I., et al., 2024. Multi-satellite data depicts record-breaking methane leak from a well blowout.
URL <https://eartharxiv.org/repository/view/6709/>
- Hasekamp, O., Lorente, A., Hu, H., Butz, A., aan de Brugh, J., Landgraf, J., 2022. Algorithm Theoretical Baseline Document for Sentinel-5 Precursor Methane Retrieval.
URL <https://sentinel.esa.int/documents/247904/2476257/Sentinel-5P-TROPOMI-ATBD-Methane-retrieval.pdf>
- Imasu, R., Matsunaga, T., Nakajima, M., Yoshida, Y., Shiomi, K., Morino, I., Saitoh, N., Niwa, Y., Someya, Y., Oishi, Y., Hashimoto, M., Noda, H., Hikosaka, K., Uchino, O., Maksyutov, S., Takagi, H., Ishida, H., Nakajima, T. Y., Nakajima, T., Shi, C., Jul 2023. Greenhouse gases observing satellite 2 (gosat-2): mission overview. *Progress in Earth and Planetary Science* 10 (1), 33.
URL <https://doi.org/10.1186/s40645-023-00562-2>
- Inoue, M., Morino, I., Uchino, O., Nakatsuru, T., Yoshida, Y., Yokota, T., Wunch, D., Wennberg, P. O., Roehl, C. M., Griffith, D. W. T., Velasco, V. A., Deutscher, N. M., Warneke, T., Notholt, J., Robinson, J., Sherlock, V., Hase, F., Blumenstock, T., Rettinger, M., Sussmann, R., Kyrö, E., Kivi, R., Shiomi, K., Kawakami, S., De Mazière, M., Arnold, S. G., Feist, D. G., Barrow, E. A., Barney, J., Dubey, M., Schneider, M., Iraci, L. T., Podolske, J. R., Hillyard, P. W., Machida, T., Sawa, Y., Tsuboi, K., Matsueda, H., Sweeney, C., Tans, P. P., Andrews, A. E., Biraud, S. C.,

- Fukuyama, Y., Pittman, J. V., Kort, E. A., Tanaka, T., 2016. Bias corrections of gosat swir xco₂ and xch₄ with tcon data and their evaluation using aircraft measurement data. *Atmospheric Measurement Techniques* 9 (8), 3491–3512.
URL <https://amt.copernicus.org/articles/9/3491/2016/>
- Irakulis-Loitxate, I., Guanter, L., Liu, Y.-N., Varon, D. J., Maasackers, J. D., Zhang, Y., Chulakadabba, A., Wofsy, S. C., Thorpe, A. K., Duren, R. M., Frankenberg, C., Lyon, D. R., Hmiel, B., Cusworth, D. H., Zhang, Y., Segl, K., Gorroño, J., Sánchez-García, E., Sulprizio, M. P., Cao, K., Zhu, H., Liang, J., Li, X., Aben, I., Jacob, D. J., 2021. Satellite-based survey of extreme methane emissions in the permian basin. *Science Advances* 7 (27).
URL <https://advances.sciencemag.org/content/7/27/eabf4507>
- Irakulis-Loitxate, I., Guanter, L., Maasackers, J. D., Zavala-Araiza, D., Aben, I., 2022. Satellites detect abatable super-emissions in one of the world's largest methane hotspot regions. *Environmental Science & Technology* 56 (4), 2143–2152, pMID: 35102741.
URL <https://doi.org/10.1021/acs.est.1c04873>
- Jacob, D. J., Varon, D. J., Cusworth, D. H., Dennison, P. E., Frankenberg, C., Gautam, R., Guanter, L., Kelley, J., McKeever, J., Ott, L. E., Poulter, B., Qu, Z., Thorpe, A. K., Worden, J. R., Duren, R. M., 2022. Quantifying methane emissions from the global scale down to point sources using satellite observations of atmospheric methane. *Atmospheric Chemistry and Physics* 22 (14), 9617–9646.
URL <https://acp.copernicus.org/articles/22/9617/2022/>
- Jervis, D., McKeever, J., Durak, B. O. A., Sloan, J. J., Gains, D., Varon, D. J., Ramier, A., Strupler, M., Tarrant, E., 2021. The ghgsat-d imaging spectrometer. *Atmospheric Measurement Techniques* 14 (3), 2127–2140.
URL <https://amt.copernicus.org/articles/14/2127/2021/>
- Jongaramrungruang, S., Thorpe, A. K., Matheou, G., Frankenberg, C., 2022. Methanet – an ai-driven approach to quantifying methane point-source emission from high-resolution 2-d plume imagery. *Remote Sensing of Environment* 269, 112809.
URL <https://www.sciencedirect.com/science/article/pii/S0034425721005290>
- Joyce, P., Ruiz Villena, C., Huang, Y., Webb, A., Gloor, M., Wagner, F. H., Chipperfield, M. P., Barrio Guilló, R., Wilson, C., Boesch, H., 2023. Using a deep neural network to detect methane point sources and quantify emissions from prisma hyperspectral satellite images. *Atmospheric Measurement Techniques* 16 (10), 2627–2640.
URL <https://amt.copernicus.org/articles/16/2627/2023/>
- Kochanov, R., Gordon, I., Rothman, L., Wcisło, P., Hill, C., Wilzewski, J., 2016. Hitran application programming interface (hapi): A comprehensive approach to working with spectroscopic data. *Journal of Quantitative Spectroscopy and Radiative Transfer* 177, 15–30, xVIIIth Symposium

- on High Resolution Molecular Spectroscopy (HighRus-2015), Tomsk, Russia.
URL <https://www.sciencedirect.com/science/article/pii/S0022407315302466>
- Koene, E. F. M., Brunner, D., Kuhlmann, G., 2024. On the theory of the divergence method for quantifying source emissions from satellite observations. *Journal of Geophysical Research: Atmospheres* 129 (12), e2023JD039904, e2023JD039904 2023JD039904.
URL <https://agupubs.onlinelibrary.wiley.com/doi/abs/10.1029/2023JD039904>
- Krings, T., Gerilowski, K., Buchwitz, M., Reuter, M., Tretner, A., Erzinger, J., Heinze, D., Pflüger, U., Burrows, J. P., Bovensmann, H., 2011. Mamap – a new spectrometer system for column-averaged methane and carbon dioxide observations from aircraft: retrieval algorithm and first inversions for point source emission rates. *Atmospheric Measurement Techniques* 4 (9), 1735–1758.
URL <https://amt.copernicus.org/articles/4/1735/2011/>
- Landgraf, J., Hasekamp, O. P., Box, M. A., Trautmann, T., 2001. A linearized radiative transfer model for ozone profile retrieval using the analytical forward-adjoint perturbation theory approach. *Journal of Geophysical Research: Atmospheres* 106 (D21), 27291–27305.
URL <https://agupubs.onlinelibrary.wiley.com/doi/abs/10.1029/2001JD000636>
- Lauvaux, T., Giron, C., Mazzolini, M., d’Aspremont, A., Duren, R., Cusworth, D., Shindell, D., Ciais, P., 2022. Global assessment of oil and gas methane ultra-emitters. *Science* 375 (6580), 557–561.
- Liu, M., van der A, R., van Weele, M., Eskes, H., Lu, X., Veefkind, P., de Laat, J., Kong, H., Wang, J., Sun, J., Ding, J., Zhao, Y., Weng, H., 2021. A new divergence method to quantify methane emissions using observations of sentinel-5p tropomi. *Geophysical Research Letters* 48 (18), e2021GL094151, e2021GL094151 2021GL094151.
URL <https://agupubs.onlinelibrary.wiley.com/doi/abs/10.1029/2021GL094151>
- Lorente, A., Borsdorff, T., Butz, A., Hasekamp, O., aan de Brugh, J., Schneider, A., Wu, L., Hase, F., Kivi, R., Wunch, D., Pollard, D. F., Shiomi, K., Deutscher, N. M., Velasco, V. A., Roehl, C. M., Wennberg, P. O., Warneke, T., Landgraf, J., 2021. Methane retrieved from TROPOMI: improvement of the data product and validation of the first 2 years of measurements. *Atmospheric Measurement Techniques* 14 (1), 665–684.
URL <https://amt.copernicus.org/articles/14/665/2021/>
- Lorente, A., Borsdorff, T., Martinez-Velarte, M. C., Landgraf, J., 2023. Accounting for surface reflectance spectral features in tropomi methane retrievals. *Atmospheric Measurement Techniques* 16 (6), 1597–1608.
URL <https://amt.copernicus.org/articles/16/1597/2023/>
- Maasackers, J. D., Omara, M., Gautam, R., Lorente, A., Pandey, S., Tol, P., Borsdorff, T., Houweling, S., Aben, I., 2022a. Reconstructing and quantifying methane emissions from the full du-
-

- ration of a 38-day natural gas well blowout using space-based observations. *Remote Sensing of Environment* 270, 112755.
URL <https://www.sciencedirect.com/science/article/pii/S0034425721004752>
- Maasackers, J. D., Varon, D. J., Elfarsdóttir, A., McKeever, J., Jervis, D., Mahapatra, G., Pandey, S., Lorente, A., Borsdorff, T., Foorhuis, L. R., Schuit, B. J., Tol, P., van Kempen, T. A., van Hees, R., Aben, I., 2022b. Using satellites to uncover large methane emissions from landfills. *Science Advances* 8 (32), eabn9683.
URL <https://www.science.org/doi/abs/10.1126/sciadv.abn9683>
- O'Dell, C. W., Eldering, A., Wennberg, P. O., Crisp, D., Gunson, M. R., Fisher, B., Frankenberg, C., Kiel, M., Lindqvist, H., Mandrake, L., Merrelli, A., Natraj, V., Nelson, R. R., Osterman, G. B., Payne, V. H., Taylor, T. E., Wunch, D., Drouin, B. J., Oyafuso, F., Chang, A., McDuffie, J., Smyth, M., Baker, D. F., Basu, S., Chevallier, F., Crowell, S. M. R., Feng, L., Palmer, P. I., Dubey, M., García, O. E., Griffith, D. W. T., Hase, F., Iraci, L. T., Kivi, R., Morino, I., Notholt, J., Ohyama, H., Petri, C., Roehl, C. M., Sha, M. K., Strong, K., Sussmann, R., Te, Y., Uchino, O., Velasco, V. A., 2018. Improved retrievals of carbon dioxide from orbiting carbon observatory-2 with the version 8 acos algorithm. *Atmospheric Measurement Techniques* 11 (12), 6539–6576.
URL <https://www.atmos-meas-tech.net/11/6539/2018/>
- Ouerghi, E., Ehret, T., Facciolo, G., Meinhardt, E., De Franchis, C., Groshenry, A., Morel, J.-M., 2024. Model adjusted matched filter for methane plume detection on prisma hyperspectral images. In: *IGARSS 2024 - 2024 IEEE International Geoscience and Remote Sensing Symposium*. pp. 8000–8004.
- Pandey, S., Gautam, R., Houweling, S., van der Gon, H. D., Sadavarte, P., Borsdorff, T., Hasekamp, O., Landgraf, J., Tol, P., van Kempen, T., Hoogeveen, R., van Hees, R., Hamburg, S. P., Maasackers, J. D., Aben, I., 2019. Satellite observations reveal extreme methane leakage from a natural gas well blowout. *Proceedings of the National Academy of Sciences* 116 (52), 26376–26381.
URL <https://www.pnas.org/doi/abs/10.1073/pnas.1908712116>
- Pandey, S., van Nistelrooij, M., Maasackers, J. D., Sutar, P., Houweling, S., Varon, D. J., Tol, P., Gains, D., Worden, J., Aben, I., 2023. Daily detection and quantification of methane leaks using sentinel-3: a tiered satellite observation approach with sentinel-2 and sentinel-5p. *Remote Sensing of Environment* 296, 113716.
URL <https://www.sciencedirect.com/science/article/pii/S0034425723002675>
- Pei, Z., Han, G., Mao, H., Chen, C., Shi, T., Yang, K., Ma, X., Gong, W., 2023. Improving quantification of methane point source emissions from imaging spectroscopy. *Remote Sensing of Environment* 295, 113652.
- Roberts, C., IJzermans, R., Randell, D., Jones, M., Jonathan, P., Mandel, K., Hirst, B., Shorttle, O., oct 2023. Avoiding methane emission rate underestimates when using the divergence

- method. *Environmental Research Letters* 18 (11), 114033.
URL <https://dx.doi.org/10.1088/1748-9326/ad0252>
- Rodgers, C. D., 2000. *Inverse Methods for Atmospheric Sounding*. WORLD SCIENTIFIC.
URL <https://www.worldscientific.com/doi/abs/10.1142/3171>
- Roger, J., Guanter, L., Gorroño, J., Irakulis-Loitxate, I., 2024a. Exploiting the entire near-infrared spectral range to improve the detection of methane plumes with high-resolution imaging spectrometers. *Atmospheric Measurement Techniques* 17 (4), 1333–1346.
URL <https://amt.copernicus.org/articles/17/1333/2024/>
- Roger, J., Irakulis-Loitxate, I., Valverde, A., Gorroño, J., Chabrilat, S., Brell, M., Guanter, L., 2024b. High-resolution methane mapping with the EnMAP satellite imaging spectroscopy mission. *IEEE Transactions on Geoscience and Remote Sensing*, 1–1.
- Rozanov, V., Buchwitz, M., Eichmann, K.-U., de Beek, R., Burrows, J., 2002. Sciatran - a new radiative transfer model for geophysical applications in the 240–2400 nm spectral region: the pseudo-spherical version. *Advances in Space Research* 29 (11), 1831–1835.
URL <https://www.sciencedirect.com/science/article/pii/S0273117702000959>
- Rozanov, V., Rozanov, A., Kokhanovsky, A., Burrows, J., 2014. Radiative transfer through terrestrial atmosphere and ocean: Software package sciatran. *Journal of Quantitative Spectroscopy and Radiative Transfer* 133, 13–71.
URL <https://www.sciencedirect.com/science/article/pii/S0022407313002872>
- Růžička, V., Mateo-García, G., Gómez-Chova, L., Vaughan, A., Guanter, L., Markham, A., 2023. Semantic segmentation of methane plumes with hyperspectral machine learning models. *Scientific Reports* 13 (1).
- Sadavarte, P., Pandey, S., Maasackers, J. D., Lorente, A., Borsdorff, T., Denier van der Gon, H., Houweling, S., Aben, I., 2021. Methane emissions from superemitting coal mines in australia quantified using tropomi satellite observations. *Environmental Science & Technology* 55 (24), 16573–16580, pMID: 34842427.
URL <https://doi.org/10.1021/acs.est.1c03976>
- Sánchez-García, E., Gorroño, J., Irakulis-Loitxate, I., Varon, D. J., Guanter, L., 2022. Mapping methane plumes at very high spatial resolution with the worldview-3 satellite. *Atmospheric Measurement Techniques* 15 (6), 1657–1674.
URL <https://amt.copernicus.org/articles/15/1657/2022/>
- Schepers, D., aan de Brugh, J., Hahne, P., Butz, A., Hasekamp, O., Landgraf, J., 2014. Lintran v2.0: A linearised vector radiative transfer model for efficient simulation of satellite-born nadir-viewing reflection measurements of cloudy atmospheres. *Journal of Quantitative Spectroscopy and Radiative Transfer* 149, 347–359.
URL <https://www.sciencedirect.com/science/article/pii/S002240731400363X>
-

Schepers, D., Guerlet, S., Butz, A., Landgraf, J., Frankenberg, C., Hasekamp, O., Blavier, J.-F., Deutscher, N. M., Griffith, D. W. T., Hase, F., Kyro, E., Morino, I., Sherlock, V., Sussmann, R., Aben, I., 2012. Methane retrievals from greenhouse gases observing satellite (gosat) short-wave infrared measurements: Performance comparison of proxy and physics retrieval algorithms. *Journal of Geophysical Research: Atmospheres* 117 (D10).

URL <https://agupubs.onlinelibrary.wiley.com/doi/abs/10.1029/2012JD017549>

Schneising, O., Buchwitz, M., Hachmeister, J., Vanselow, S., Reuter, M., Buschmann, M., Bovensmann, H., Burrows, J. P., 2023. Advances in retrieving xch_4 and xco from sentinel-5 precursor: improvements in the scientific tropomi/wfmd algorithm. *Atmospheric Measurement Techniques* 16 (3), 669–694.

URL <https://amt.copernicus.org/articles/16/669/2023/>

Schneising, O., Buchwitz, M., Reuter, M., Bovensmann, H., Burrows, J. P., Borsdorff, T., Deutscher, N. M., Feist, D. G., Griffith, D. W. T., Hase, F., Hermans, C., Iraci, L. T., Kivi, R., Landgraf, J., Morino, I., Notholt, J., Petri, C., Pollard, D. F., Roche, S., Shiomi, K., Strong, K., Sussmann, R., Velazco, V. A., Warneke, T., Wunch, D., 2019. A scientific algorithm to simultaneously retrieve carbon monoxide and methane from tropomi onboard sentinel-5 precursor. *Atmospheric Measurement Techniques* 12 (12), 6771–6802.

URL <https://amt.copernicus.org/articles/12/6771/2019/>

Schneising, O., Buchwitz, M., Reuter, M., Vanselow, S., Bovensmann, H., Burrows, J. P., 2020. Remote sensing of methane leakage from natural gas and petroleum systems revisited. *Atmospheric Chemistry and Physics* 20 (15), 9169–9182.

URL <https://acp.copernicus.org/articles/20/9169/2020/>

Schuit, B. J., Maasackers, J. D., Bijl, P., Mahapatra, G., Van den Berg, A.-W., Pandey, S., Lorente, A., Borsdorff, T., Houweling, S., Varon, D. J., McKeever, J., Jervis, D., Girard, M., Irakulis-Loitxate, I., Gorroño, J., Guanter, L., Cusworth, D. H., Aben, I., 2023. Automated detection and monitoring of methane super-emitters using satellite data. *Atmospheric Chemistry and Physics Discussions* 2023, 1–47.

URL <https://acp.copernicus.org/preprints/acp-2022-862/>

Sherwin, E. D., El Abbadi, S. H., Burdeau, P. M., Zhang, Z., Chen, Z., Rutherford, J. S., Chen, Y., Brandt, A. R., 2024. Single-blind test of nine methane-sensing satellite systems from three continents. *Atmospheric Measurement Techniques* 17 (2), 765–782.

URL <https://amt.copernicus.org/articles/17/765/2024/>

Sherwin, E. D., Rutherford, J. S., Chen, Y., Aminfar, S., Kort, E. A., Jackson, R. B., Brandt, A. R., 2023. Single-blind validation of space-based point-source detection and quantification of onshore methane emissions. *Scientific Reports* 13, 3836.

URL <https://amt.copernicus.org/articles/11/5673/2018/>

- Stein, A. F., Draxler, R. R., Rolph, G. D., Stunder, B. J. B., Cohen, M. D., Ngan, F., 2015. Noaa's hysplit atmospheric transport and dispersion modeling system. *Bulletin of the American Meteorological Society* 96 (12), 2059 – 2077.
URL <https://journals.ametsoc.org/view/journals/bams/96/12/bams-d-14-00110.1.xml>
- Thompson, D. R., Leifer, I., Bovensmann, H., Eastwood, M., Fladeland, M., Frankenberg, C., Gerilowski, K., Green, R. O., Kratwurst, S., Krings, T., Luna, B., Thorpe, A. K., 2015. Real-time remote detection and measurement for airborne imaging spectroscopy: a case study with methane. *Atmospheric Measurement Techniques* 8 (10), 4383–4397.
URL <https://amt.copernicus.org/articles/8/4383/2015/>
- Thompson, D. R., Thorpe, A. K., Frankenberg, C., Green, R. O., Duren, R., Guanter, L., Hollstein, A., Middleton, E., Ong, L., Ungar, S., 2016. Space-based remote imaging spectroscopy of the aliso canyon ch4 superemitter. *Geophysical Research Letters* 43 (12), 6571–6578.
URL <https://agupubs.onlinelibrary.wiley.com/doi/abs/10.1002/2016GL069079>
- Thorpe, A. K., Frankenberg, C., Roberts, D. A., 2014. Retrieval techniques for airborne imaging of methane concentrations using high spatial and moderate spectral resolution: application to aviris. *Atmospheric Measurement Techniques* 7 (2), 491–506.
URL <https://amt.copernicus.org/articles/7/491/2014/>
- Thorpe, A. K., Frankenberg, C., Thompson, D. R., Duren, R. M., Aubrey, A. D., Bue, B. D., Green, R. O., Gerilowski, K., Krings, T., Borchardt, J., Kort, E. A., Sweeney, C., Conley, S., Roberts, D. A., Dennison, P. E., 2017. Airborne doas retrievals of methane, carbon dioxide, and water vapor concentrations at high spatial resolution: application to aviris-ng. *Atmospheric Measurement Techniques* 10 (10), 3833–3850.
URL <https://amt.copernicus.org/articles/10/3833/2017/>
- Thorpe, A. K., Green, R. O., Thompson, D. R., Brodrick, P. G., Chapman, J. W., Elder, C. D., Irakulis-Loitxate, I., Cusworth, D. H., Ayasse, A. K., Duren, R. M., Frankenberg, C., Guanter, L., Worden, J. R., Dennison, P. E., Roberts, D. A., Chadwick, K. D., Eastwood, M. L., Fahlen, J. E., Miller, C. E., 2023. Attribution of individual methane and carbon dioxide emission sources using EMIT observations from space. *Science Advances* 9 (46), eadh2391.
- Tu, Q., Hase, F., Qin, K., Cohen, J. B., Khosrawi, F., Zou, X., Schneider, M., Lu, F., 2024. Quantifying ch₄ emissions from coal mine aggregation areas in shanxi, china, using tropomi observations and the wind-assigned anomaly method. *Atmospheric Chemistry and Physics* 24 (8), 4875–4894.
URL <https://acp.copernicus.org/articles/24/4875/2024/>
- Tu, Q., Hase, F., Schneider, M., García, O., Blumenstock, T., Borsdorff, T., Frey, M., Khosrawi, F., Lorente, A., Alberti, C., Bustos, J. J., Butz, A., Carreño, V., Cuevas, E., Curcoll, R., Diekmann,

- C. J., Dubravica, D., Ertl, B., Estruch, C., León-Luis, S. F., Marrero, C., Morgui, J.-A., Ramos, R., Scharun, C., Schneider, C., Sepúlveda, E., Toledano, C., Torres, C., 2022a. Quantification of ch_4 emissions from waste disposal sites near the city of Madrid using ground- and space-based observations of COCON, IASI. *Atmospheric Chemistry and Physics* 22 (1), 295–317.
URL <https://acp.copernicus.org/articles/22/295/2022/>
- Tu, Q., Schneider, M., Hase, F., Khosrawi, F., Ertl, B., Necki, J., Dubravica, D., Diekmann, C. J., Blumenstock, T., Fang, D., 2022b. Quantifying ch_4 emissions in hard coal mines from Tropomi and IASI observations using the wind-assigned anomaly method. *Atmospheric Chemistry and Physics* 22 (15), 9747–9765.
URL <https://acp.copernicus.org/articles/22/9747/2022/>
- Vanselow, S., Schneising, O., Buchwitz, M., Reuter, M., Bovensmann, H., Boesch, H., Burrows, J. P., 2024. Automated detection of regions with persistently enhanced methane concentrations using Sentinel-5 Precursor satellite data. *EGU Sphere* 2024, 1–43.
URL <https://egusphere.copernicus.org/preprints/2024/egusphere-2024-379/>
- Varon, D. J., Jacob, D. J., Jervis, D., McKeever, J., 2020. Quantifying Time-Averaged Methane Emissions from Individual Coal Mine Vents with GHGSat-D Satellite Observations. *Environmental Science & Technology* 54 (16), 10246–10253, PMID: 32672947.
URL <https://doi.org/10.1021/acs.est.0c01213>
- Varon, D. J., Jacob, D. J., McKeever, J., Jervis, D., Durak, B. O. A., Xia, Y., Huang, Y., 2018. Quantifying methane point sources from fine-scale satellite observations of atmospheric methane plumes. *Atmospheric Measurement Techniques* 11 (10), 5673–5686.
URL <https://amt.copernicus.org/articles/11/5673/2018/>
- Varon, D. J., Jervis, D., McKeever, J., Spence, I., Gains, D., Jacob, D. J., 2021. High-frequency monitoring of anomalous methane point sources with multispectral Sentinel-2 satellite observations. *Atmospheric Measurement Techniques* 14 (4), 2771–2785.
URL <https://amt.copernicus.org/articles/14/2771/2021/>
- Varon, D. J., McKeever, J., Jervis, D., Maasackers, J. D., Pandey, S., Houweling, S., Aben, I., Scarpelli, T., Jacob, D. J., 2019. Satellite Discovery of Anomalously Large Methane Point Sources From Oil/Gas Production. *Geophysical Research Letters* 46 (22), 13507–13516.
URL <https://agupubs.onlinelibrary.wiley.com/doi/abs/10.1029/2019GL083798>
- Vaughan, A., Mateo-García, G., Gómez-Chova, L., Růžička, V., Guanter, L., Irakulis-Loitxate, I., 2024. CH4net: a deep learning model for monitoring methane super-emitters with Sentinel-2 imagery. *Atmospheric Measurement Techniques* 17 (9), 2583–2593.
URL <https://amt.copernicus.org/articles/17/2583/2024/>
- Veefkind, J. P., Serrano-Calvo, R., de Gouw, J., Dix, B., Schneising, O., Buchwitz, M., Barré, J., van der A, R. J., Liu, M., Levelt, P. F., 2023. Widespread frequent methane emissions from

the oil and gas industry in the permian basin. *Journal of Geophysical Research: Atmospheres* 128 (3), e2022JD037479, e2022JD037479 2022JD037479.

URL <https://agupubs.onlinelibrary.wiley.com/doi/abs/10.1029/2022JD037479>

Watine-Guiu, M., Varon, D. J., Irakulis-Loitxate, I., Balasus, N., Jacob, D. J., 2023. Geostationary satellite observations of extreme and transient methane emissions from oil and gas infrastructure. *Proceedings of the National Academy of Sciences* 120 (52), e2310797120.

URL <https://www.pnas.org/doi/abs/10.1073/pnas.2310797120>

White, W. H., Anderson, J. A., Blumenthal, D. L., Husar, R. B., Gillani, N. V., Husar, J. D., Wilson, W. E., 1976. Formation and transport of secondary air pollutants: Ozone and aerosols in the st. louis urban plume. *Science* 194 (4261), 187–189.

URL <https://www.science.org/doi/abs/10.1126/science.959846>

Wu, L., Hasekamp, O., Hu, H., Landgraf, J., Butz, A., aan de Brugh, J., Aben, I., Pollard, D. F., Griffith, D. W. T., Feist, D. G., Koshelev, D., Hase, F., Toon, G. C., Ohyama, H., Morino, I., Notholt, J., Shiomi, K., Iraci, L., Schneider, M., de Mazière, M., Sussmann, R., Kivi, R., Warneke, T., Goo, T.-Y., Té, Y., 2018. Carbon dioxide retrieval from oco-2 satellite observations using the remotec algorithm and validation with tcon measurements. *Atmospheric Measurement Techniques* 11 (5), 3111–3130.

URL <https://www.atmos-meas-tech.net/11/3111/2018/>

Wunch, D., Toon, G. C., Blavier, J.-F. L., Washenfelder, R. A., Notholt, J., Connor, B. J., Griffith, D. W. T., Sherlock, V., Wennberg, P. O., 2011. The total carbon column observing network. *Philosophical Transactions of the Royal Society A: Mathematical, Physical and Engineering Sciences* 369 (1943), 2087–2112.

URL <https://royalsocietypublishing.org/doi/abs/10.1098/rsta.2010.0240>

Zhang, Y., Gautam, R., Pandey, S., Omara, M., Maasackers, J. D., Sadavarte, P., Lyon, D., Nesser, H., Sulprizio, M. P., Varon, D. J., Zhang, R., Houweling, S., Zavala-Araiza, D., Alvarez, R. A., Lorente, A., Hamburg, S. P., Aben, I., Jacob, D. J., 2020. Quantifying methane emissions from the largest oil-producing basin in the united states from space. *Science Advances* 6 (17), eaaz5120.

URL <https://www.science.org/doi/abs/10.1126/sciadv.aaz5120>